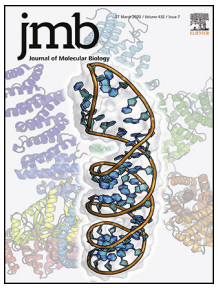

Sclerotiorin Stabilizes the Assembly of Nonfibrillar Abeta42 Oligomers with Low Toxicity, Seeding Activity, and Beta-sheet Content

Thomas Wiglenda[1,†], Nicole Groenke[1,†], Waldemar Hoffmann[2], Christian Manz[2], Lisa Diez[1], Alexander Buntru[1], Lydia Brusendorf[1], Nancy Neuendorf[1], Sigrid Schnoegl[1], Christian Haenig[1], Peter Schmieder[3], Kevin Pagel[2] and Erich E. Wanker[1]

*1 - **Neuroproteomics,** Max Delbrück Center for Molecular Medicine in the Helmholtz Association, Berlin, Germany*
*2 - **Institut für Chemie und Biochemie,** Freie Universität Berlin, Berlin, Germany*
*3 - **Leibniz-Institut für Molekulare Pharmakologie,** Berlin, Germany*

***Correspondence to Erich E. Wanker:** Max Delbrück Center for Molecular Medicine (MDC) in the Helmholtz Association, Robert-Roessle-Strasse 10, 13125, Berlin, Germany, Fax: +49 30 9406-2552. ewanker@mdc-berlin.de*
https://doi.org/10.1016/j.jmb.2020.01.033
Edited by Ronald Wetzel.

Abstract

The self-assembly of the 42-residue amyloid-β peptide, Aβ42, into fibrillar aggregates is associated with neuronal dysfunction and toxicity in Alzheimer's disease (AD) patient brains, suggesting that small molecules acting on this process might interfere with pathogenesis. Here, we present experimental evidence that the small molecule sclerotiorin (SCL), a natural product belonging to the group of azaphilones, potently delays both seeded and nonseeded Aβ42 polymerization in cell-free assays. Mechanistic biochemical studies revealed that the inhibitory effect of SCL on fibrillogenesis is caused by its ability to kinetically stabilize small Aβ42 oligomers. These structures exhibit low β-sheet content and do not possess seeding activity, indicating that SCL acts very early in the amyloid formation cascade before the assembly of seeding-competent, β-sheet-rich fibrillar aggregates. Investigations with NMR WaterLOGSY experiments confirmed the association of Aβ42 assemblies with SCL in solution. Furthermore, using ion mobility-mass spectrometry, we observed that SCL directly interacts with a small fraction of Aβ42 monomers in the gas phase. In comparison to typical amyloid fibrils, small SCL-stabilized Aβ42 assemblies are inefficiently taken up into mammalian cells and have low toxicity in cell-based assays. Overall, these mechanistic studies support a pathological role of stable, β-sheet-rich Aβ42 fibrils in AD, while structures with low β-sheet content may be less relevant.

Introduction

Alzheimer's disease (AD) is a late-onset neurodegenerative disorder characterized by memory loss and progressive personality changes [1,2]. The self-assembly of the 42-residue amyloid-β (Aβ42) peptide, produced by proteolytic cleavage of the amyloid-β precursor protein (APP), into insoluble fibrillar structures in AD patient brains is regarded as one critical, possibly the key feature of pathogenesis [3,4].

Various studies suggest that not only mature amyloid fibrils but also small soluble Aβ42 oligomers lead to disease phenotypes and neuronal dysfunction [5] and cause toxicity in various cellular models [6–8]. Whether ordered amyloid fibrils or unstructured prefibrillar oligomers are the major toxic agent in disease, however, is still a matter of intense debate [9].

Previous investigations with synthetic or recombinant peptides have demonstrated that unstructured

Aβ42 monomers self-assemble into ordered, β-sheet-rich amyloid fibrils by a nucleation-dependent process [3,10] that is accelerated by the addition of preformed amyloid fibrils, often termed "seeds" [4]. The formation of Aβ42 fibrils is a complex, multistep autocatalytic process, involving the assembly of transient on- and off-pathway aggregate species, whose structures, sizes, and biological activities are not well defined [11]. Therefore, clarifying the roles of transiently formed oligomers and other prefibrillar structures in pathogenesis is highly relevant to defining viable therapeutic strategies.

Several lines of experimental evidence indicate that amyloid formation pathways can be manipulated with chemical compounds [12], peptides [13], or larger proteins acting as molecular chaperones [14]. Organic dyes like Congo red [15] and K114 [16] or polyphenols like EGCG [17], which directly bind to ordered β-sheet-rich amyloid structures, have been shown to slow down fibrillogenesis when added to complex Aβ42 polymerization reactions. Furthermore, it was demonstrated that the chaperone Brichos, a protein domain of ~100 amino acids that directly binds to the surface of amyloid fibrils [18], can efficiently inhibit the assembly of Aβ42 oligomers, which are formed by secondary nucleation. Thus, small molecules or proteins that interfere with surface-catalyzed Aβ42 secondary nucleation might have a high therapeutic potential for the treatment of AD and other protein misfolding disorders.

If small β-sheet-rich, seeding-competent Aβ42 assemblies are the major toxic species in AD, no matter whether oligomers or fibrils, inhibition of their formation with small molecules should reduce toxicity. This could be achieved with chemical compounds that preferentially target unstructured Aβ42 monomers or oligomers and prevent their conformational conversion into β-sheet-rich, aggregation-prone structures. A compound that successfully stabilizes the conformation of the protein transthyretin and prevents its spontaneous misfolding and aggregation has been developed for clinical use and is now applied for the treatment of patients of TTR amyloidosis [19,20].

Here, we searched for chemical compounds that interfere with early events in the Aβ42 aggregation cascade and prevent the assembly of potentially proteotoxic, β-sheet-rich structures. We identified the natural compound sclerotiorin (SCL) and showed that it kinetically stabilizes small nonseeding-competent oligomers with a low β-sheet-content, indicating that it interferes with very early steps in the amyloid polymerization process. NMR WaterLOGSY experiments indicate that SCL interacts with newly formed Aβ42 assemblies, confirming its direct binding to the aggregation-prone peptide. Finally, we observed that SCL-stabilized oligomers in comparison to amyloid fibrils are inefficiently taken up into mammalian cells and exhibit low toxicity in cell-based assays. Together, these studies indicate that SCL perturbs very early events in the amyloid formation cascade and stabilizes the assembly of benign, unstructured Aβ42 oligomers with low SDS stability. The potential implications of these results for the treatment of AD and other amyloid diseases are discussed.

Results

The natural compound SCL potently delays both seed-mediated and spontaneous Aβ42 polymerization in FP and ThT assays

We used a fluorescence polarization (FP)-based assay to screen for small molecules that delay seed-mediated Aβ42 aggregation *in vitro* (fig. S1a). In this assay, FP is used to monitor the time-dependent co-aggregation of 5-Carboxyfluorescin-conjugated tracer peptides (^{FAM}Aβ42, 0.1 μM) and unlabeled Aβ42 peptides (10 μM) into higher molecular weight fibrillar structures [21]. Small, preformed, β-sheet-rich Aβ42 fibrils are utilized in this method as seeds to promote amyloid fibrillogenesis (fig. S1b). We screened a focused library of 502 natural compounds for their potency to delay seed-mediated ^{FAM}Aβ42/Aβ42 copolymerization. The compounds were added to reactions at substoichiometric concentrations (2 μM) to avoid unspecific effects through abnormal compound aggregation, which is often observed at higher concentrations [22].

Using this approach, we found that the natural compounds, epigallocatechin gallate (EGCG), wedelolactone (WED) and α-apo-oxytetracycline (αOXY) potently delay the onset of seed-mediated ^{FAM}Aβ42/Aβ42 copolymerization in FP assays (Fig. 1a and b), confirming previous results that polyphenols and tetracyclines can slow down amyloid fibrillogenesis [23,24]. Strikingly, an even stronger effect on seed-mediated ^{FAM}Aβ42/Aβ42 co-aggregation was observed with the small molecule sclerotiorin (SCL), a chlorine-containing azaphilone-type natural product [25]. It was first isolated in 1940 from *Penicillium sclerotiorum* [26]. SCL has antifungal activity [27] but also inhibits 5-lipoxygenase activity and platelet aggregation [28]. An effect on Aβ42 aggregation in the context of AD, however, has not been described.

The inhibitory effects of the compounds were confirmed when they were added to ^{FAM}Aβ42/Aβ42 co-aggregation reactions in the absence of preformed seeds (Fig. 1c). Under these experimental conditions, a substoichiometric concentration of the compound SCL prevented the time-dependent appearance of FP for 15 h, while in the presence of the compounds EGCG, WED, or αOXY, FP

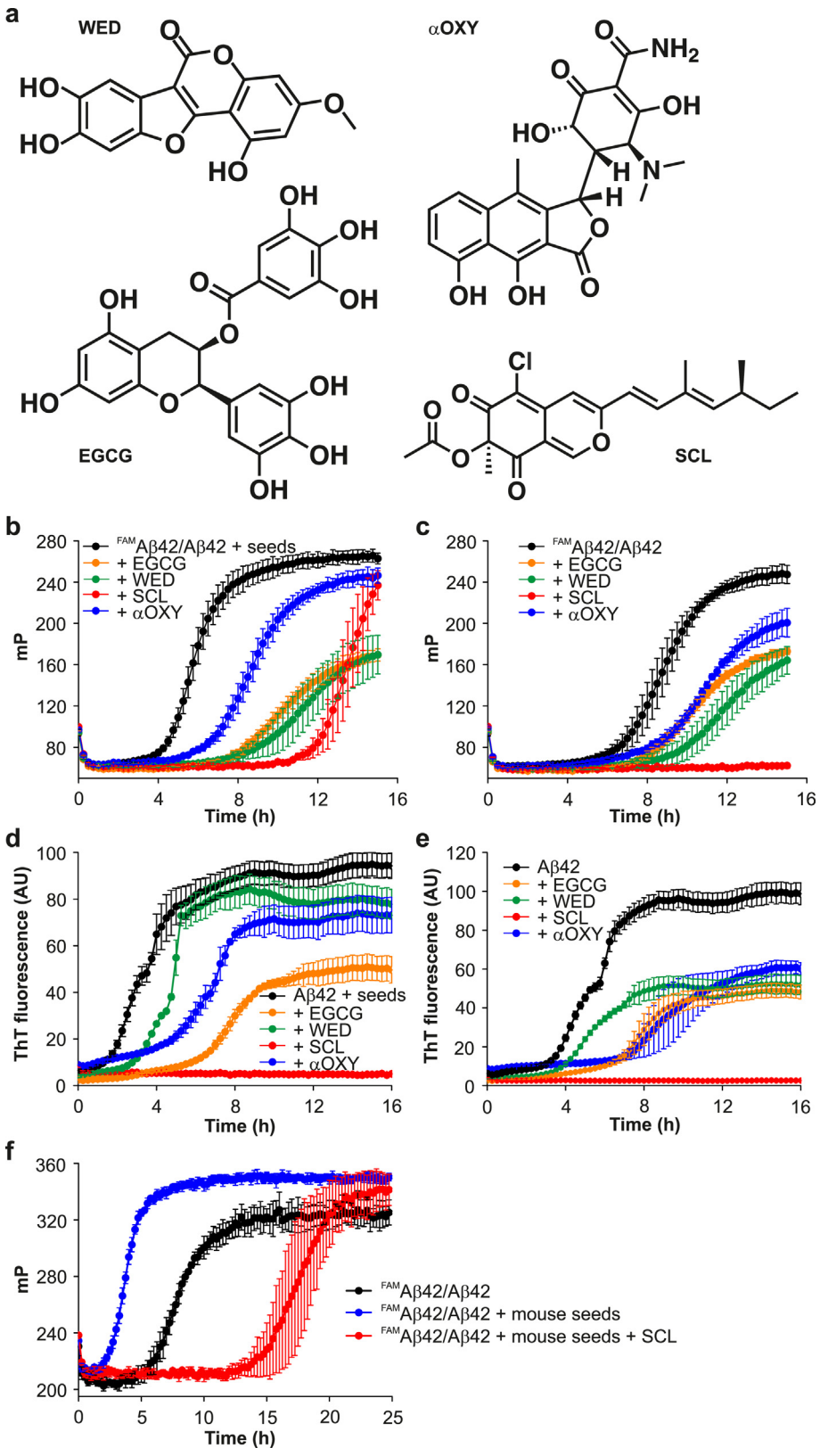
a
WED
αOXY
EGCG
SCL
b
FAMAβ42/Aβ42 + seeds
+ EGCG
+ WED
+ SCL
+ αOXY
mP
Time (h)
c
FAMAβ42/Aβ42
+ EGCG
+ WED
+ SCL
+ αOXY
mP
Time (h)
d
ThT fluorescence (AU)
Aβ42 + seeds
+ EGCG
+ WED
+ SCL
+ αOXY
Time (h)
e
ThT fluorescence (AU)
Aβ42
+ EGCG
+ WED
+ SCL
+ αOXY
Time (h)
f
mP
FAMAβ42/Aβ42
FAMAβ42/Aβ42 + mouse seeds
FAMAβ42/Aβ42 + mouse seeds + SCL
Time (h)

started to increase after ~8 h (Fig. 1c). Next, we directly compared the potencies of the compounds EGCG, WED, αOXY, and SCL in a time-resolved Thioflavin T (ThT) aggregation assay [29]. In this case, the compounds (10 μM) were incubated in the presence and absence of preformed Aβ42 seeds (250 nM) with Aβ42 monomers (25 μM) and ThT (25 μM). Fibrillogenesis of Aβ42 peptides was monitored by quantification of ThT fluorescence emission at 485 nm over time. We again observed that SCL delays Aβ42 polymerization more potently than WED, αOXY, and EGCG (Fig. 1d and e), confirming the results obtained with FP assays (Fig. 1b and c).

Finally, we addressed the question of whether SCL can influence the seeding activity of Aβ aggregates that are formed in the brains of AD transgenic mice. In previous studies, fibrillar Aβ aggregates have been detected in the 5 × FAD mouse model [30]. Here, we isolated such structures from APPPS1 mouse brain tissues [31]. Brain extracts were first immunoprecipitated with beads using the monoclonal anti-Aβ antibody 6E10. Then, the immunoprecipitates were released from the beads by sonication and analyzed by SDS-PAGE and immunoblotting, as well as staining of gels with Coomassie blue R. We found that both high molecular weight Aβ aggregates and monomers were very specifically enriched from mouse brain extracts by the anti-Aβ antibody 6E10 but not by the isogenic control antibody (fig. S2a,b). Finally, the enriched Aβ structures were added as seeds to fluorescently labeled and unlabeled Aβ42 monomers in FP assays. We observed that the immunoprecipitated Aβ aggregates prepared from APPPS1 transgenic mice are indeed seeding-competent structures and potently decrease the lag phase in ^{FAM}Aβ42/Aβ42 co-aggregation reactions (Fig. 1f). This effect, however, was diminished when SCL (2 μM) was added to FP reactions together with the immunoprecipitated Aβ seeds. Based on the evidence that SCL influences the seeding activity of Aβ aggregates enriched from AD transgenic mice, we continued with a more detailed mechanistic investigation of the compound.

SCL slows fibrillogenesis by stabilizing small, nonfibrillar Aβ42 assemblies

To study how SCL influences amyloid aggregation, we first analyzed the time-dependent formation of ^{FAM}Aβ42/Aβ42 co-assemblies in the presence and absence of the compound (10 μM) by blue native (BN) PAGE and immunoblotting. In the absence of SCL, we observed a rapid increase of high-molecular-weight Aβ42 assemblies (HMWAs) in the gel pockets (Fig. 2a), confirming previous observations that Aβ42 peptides efficiently convert into high-molecular-weight aggregates in cell-free assays [23]. Interestingly, the formation of HMWAs was delayed for more than 10 h in the presence of SCL, demonstrating that the compound interferes with early events in the aggregation cascade and slows down the assembly of large structures. Concomitantly with a decrease of HMWAs in SCL-treated samples, however, an increase of lower-molecular-weight Aβ42 assemblies (LMWAs) migrating at ~70−500 kDa was observed (Fig. 2a), indicating that the compound stabilizes small Aβ42 oligomers in the aggregation cascade. A similar result was obtained when seeded Aβ42 aggregation reactions were treated with the chemical compound and analyzed by BN-PAGE and immunoblotting (fig. S2c).

Next, we applied a native filter retardation assay (nFRA) to assess the impact of SCL on the self-assembly of Aβ42 aggregates. With this method, the formation of large, stable amyloid aggregates but not monomers or small oligomers can be detected and quantified in complex polymerization reactions [32]. We observed that upon SCL treatment (10 μM) the time-dependent formation of large Aβ42 aggregates was delayed considerably (Fig. 2b and c), confirming the results obtained by BN-PAGE and immunoblotting (Fig. 2a).

We also studied the morphology of Aβ42 aggregates in SCL-treated and untreated reactions by electron microscopy (EM). We treated Aβ42 monomers (10 μM) with preformed seeds (100 nM) and an equimolar concentration of SCL and analyzed the reactions after incubation for 15 h at 37 °C. In comparison to untreated samples, the abundance of small spherical oligomers was increased in SCL-

Fig. 1. Effects of small molecules on both spontaneous and seed-mediated Aβ42 aggregation in FP and ThT assays. (**a**) Structures of the tested small molecules Wedelolactone (WED), α-apo-Oxytetracycline (α-OXY), Epigallocatechin gallate (EGCG) and Sclerotiorin (SCL). (**b, c**) Effects of chemical compounds on seed-mediated (**b**) and spontaneous (**c**) coaggregation of ^{FAM}Aβ42 (0.1 μM) and Aβ42 (10 μM) peptides in FP assays. Preformed β-sheet-rich fibrillar assemblies (100 nM monomer equivalent) were added as seeds. mP, milli-polarization units (**d, e**) Effects of chemical compounds on seed-mediated (**d**) and spontaneous (**e**) aggregation of Aβ42 (25 μM) peptides in Thioflavin T (ThT, 25 μM) dye-binding assays. Preformed β-sheet-rich Aβ42 fibrils (250 nM monomer equivalent) were added as seeds. (**f**) SCL (2 μM) decreases the seeding activity of fibrillar Aβ aggregates prepared from the brains of 5xFAD transgenic mice in FP assays. Aβ aggregates were immunoprecipitated from mouse brain extracts using the 6E10 antibody. Coaggregation of ^{FAM}Aβ42 (0.1 μM) and Aβ42 (10 μM) peptides was monitored in FP assays. mP, milli-polarization units (**b**–**f**) Values are means ± SD, n = 4.

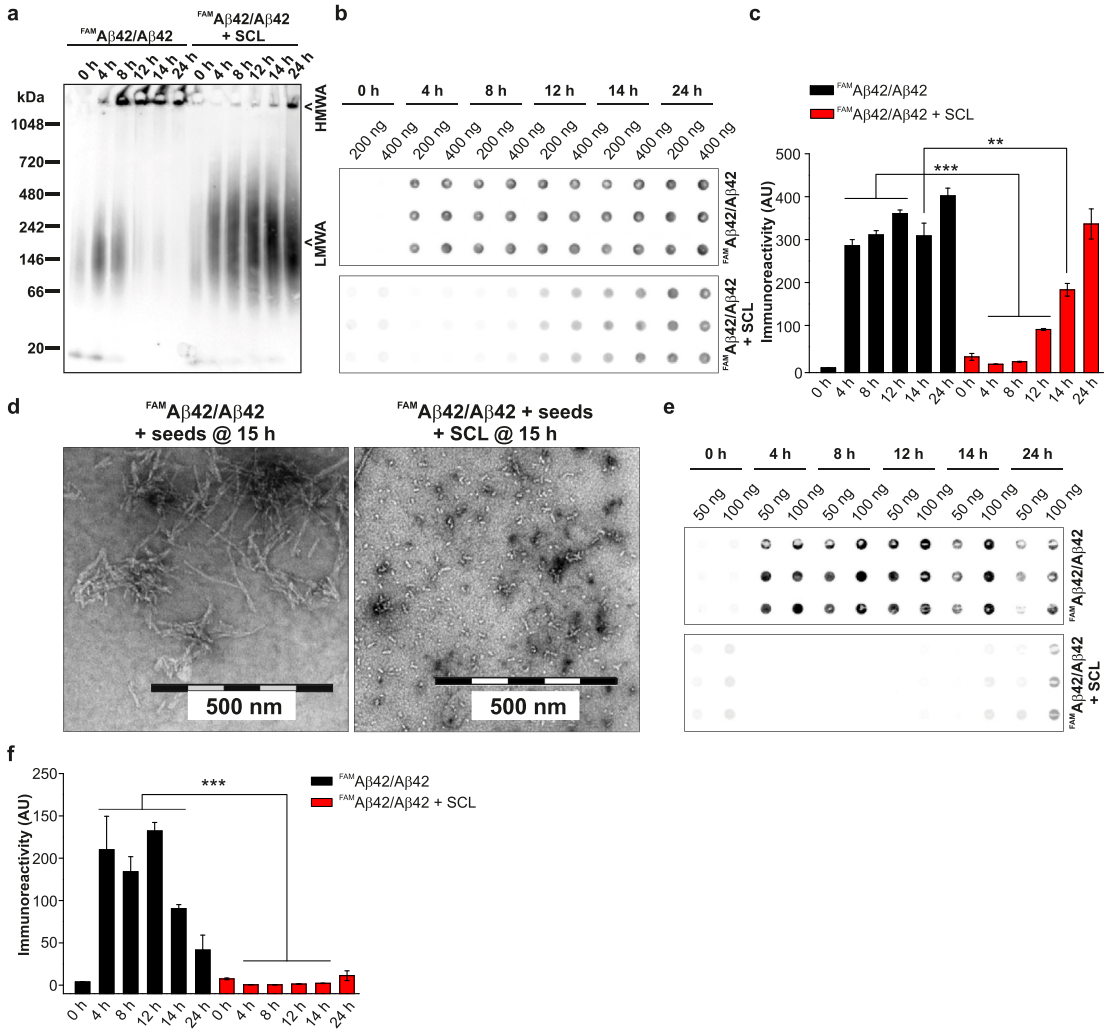

Fig. 2. SCL slows down fibrillogenesis by stabilizing small, nonfibrillar Aβ42 assemblies. (**a**) Analysis of SCL-treated (10 μM) and untreated ^{FAM}Aβ42/Aβ42 (0.1/10 μM) coaggregation reactions by blue native (BN) PAGE and immunoblotting using the 6E10 antibody. (**b**) Detection of ^{FAM}Aβ42/Aβ42 (0.1/10 μM) coaggregation by native filter retardation assay (nFRA). SCL-treated (lower panel, 10 μM) and untreated reactions were analyzed. Aggregates retained on filter membranes detected with 6E10 antibody. (**c**) Quantification of immunoreactive material on the filter membrane shown in **b**. (**d**) Electron microscopy analysis of seeded (100 nM seeds) ^{FAM}Aβ42/Aβ42 coaggregation reactions (0.1/10 μM) in the absence and presence of SCL (10 μM) after 15 h. Seeds were prepared from synthetic Aβ42 peptides (see Fig. 1b). (**e**) Investigation of SCL-treated (lower panel, 10 μM) and untreated (upper panel) ^{FAM}Aβ42/Aβ42 (0.1/10 μM) coaggregation reactions by dot blot assays using the fibril-specific 352 antibody. (**f**) Quantification of immunoreactive material shown in **e.** In **b**, **c**, **e,** and **f,** values are means ± SD, n = 3. Asterisks indicate significant differences as determined by the student *t*-test: * ≤0.05, ** ≤0.01, *** ≤0.001.

treated reactions (Fig. 2d), substantiating the results with BN-PAGE and immunoblotting that the compound acts early in the aggregation cascade and stabilizes small Aβ42 assemblies. Similar results were obtained when SCL-treated Aβ42 aggregation reactions in the presence of preformed seeds were analyzed with AFM after 15 h (fig. S2d).

Finally, to quantify the formation of fibrillar Aβ42 aggregates in SCL-treated and untreated reactions, we performed dot blot assays using the monoclonal anti-Aβ antibody 352. This antibody specifically recognizes large ThT-reactive, fibrillar Aβ42 aggregates in dot blot assays, while unstructured monomers and small oligomers are not detected (fig. S3a-c). We found that, in comparison to controls, SCL treatment efficiently delays the time-dependent appearance of antibody 352 immunoreactivity in Aβ42 polymerization reactions (Fig. 2e and f), confirming our observations by EM (Fig. 2d) that the compound potently inhibits the formation of large

fibrillar Aβ42 aggregates. Together, this indicates that SCL perturbs early events in the fibril assembly process and kinetically stabilizes small Aβ42 oligomers prior to their conversion into large, fibrillar structures.

SCL-stabilized Aβ42 assemblies are structures with low SDS stability and β-sheet content

For assessing the stability of the small SCL-stabilized Aβ42 assemblies, we analyzed the time-dependent formation of amyloid aggregates in SCL-treated (10 μM) and untreated reactions by SDS-PAGE and immunoblotting. In untreated reactions, SDS-stable HMWAs were predominantly detected from ~4 h onward (Fig. 3a), indicating that in the absence of the chemical compound, unstructured Aβ42 monomers rapidly self-assemble into large, SDS-stable structures. However, SDS-stable HMWAs were undetectable in SCL-treated reactions. This indicates that the LMWAs and the HMWAs observed in native gels in the presence of SCL (Fig. 2a) are less stable structures, which disassemble upon treatment with SDS into monomers and very low molecular weight oligomers (Fig. 3a). This result was confirmed when time-resolved SCL-treated and untreated Aβ42 aggregation reactions were systematically analyzed using a denaturing filter retardation assay (dFRA), which exclusively detects large, SDS- and heat-stable Aβ42 aggregates retained on filter membranes (fig. S4a,b).

We next investigated the impact of SCL treatment on the time-dependent formation of Aβ42 assemblies by circular dichroism (CD) spectroscopy. With this method, potential changes in the secondary structure of spontaneously formed Aβ42 aggregates can be elucidated [17]. In comparison to untreated controls (Fig. 3b), the β-sheet-content in SCL-treated reactions was decreased (Fig. 3c), confirming our hypothesis that the small compound-stabilized Aβ42 structures (Fig. 2a) are structurally distinct from typical, ordered amyloid fibrils with a high β-sheet content [23].

A similar result was obtained when SCL-treated and untreated Aβ42 assemblies were analyzed with the fluorescent dye ThT, which preferentially binds to ordered amyloid fibrils with a high β-sheet-content [33]. We treated Aβ42 monomers (25 μM) with increasing concentrations of SCL and incubated the reactions for 15 h at 37 °C in order to stimulate aggregate formation. Then, the dye ThT (25 μM) was added to reactions, and fluorescence emission was quantified at 485 nm. In comparison to untreated control reactions, we observed significantly decreased ThT fluorescence in SCL-treated samples (fig. S5), supporting the hypothesis that the compound-stabilized LMWAs in native gels (Fig. 2a) are structures with low β-sheet content.

Finally, we investigated whether SCL treatment influences the binding of the fluorescent dye 8-Anilino-1-naphthalene sulfonic acid (ANS) to spontaneously formed Aβ42 assemblies. ANS was previously shown to interact with fibrillar, β-sheet-rich Aβ42 aggregates [34], suggesting that SCL treatment should decrease ANS fluorescence if it prevents the formation of fibrillar structures. We treated Aβ42 monomers (20 μM) with an equal concentration of SCL and incubated the reaction for 24 h at 37 °C. Then, ANS was added, and emission spectra between 380 and 650 nm were recorded using a constant excitation wavelength of 350 nm. A high emission peak with a maximum wavelength of ~500 nm was detectable in untreated samples (Fig. 3d), confirming the formation of fibrillar Aβ42 aggregates with solvent-exposed hydrophobic clusters. In comparison, ANS fluorescence emission at ~500 nm was decreased in SCL-treated samples, substantiating results obtained with CD measurements (Fig. 3b and c) and ThT-binding assays (fig. S5) that the compound delays the formation of fibrillar, β-sheet-rich Aβ42 aggregates.

SCL-stabilized Aβ42 assemblies are nonseeding-competent structures

Our studies indicate that SCL interferes with very early steps in the Aβ42 aggregation cascade and leads to the stabilization of small structures with low β-sheet content and a low propensity to form fibrillar aggregates. This suggests that the compound-stabilized Aβ42 assemblies observed in native gels (Fig. 2a) are structures with low seeding activity. For addressing this question, we first produced Aβ42 assemblies in the presence and absence of SCL. Aβ42 monomers (10 μM) were incubated with an equal concentration of SCL for 18 h at 37 °C in order to obtain higher molecular weight aggregates. Then, these structures were added as seeds (100 nM) to FP-based aggregation assays in 384-well microtiter plates to monitor their seeding activity (fig. S6a). We observed a significant shortening of the lag phase, when Aβ42 aggregates formed in the absence of SCL were added to ^{FAM}Aβ42/Aβ42 copolymerization assays (Fig. 3e and f), indicating that spontaneously formed Aβ42 aggregates possess seeding activity. Strikingly, such an effect was not observed when SCL-treated samples were added to FP assays, demonstrating that the small SCL-stabilized Aβ42 oligomers observed in native gels (Fig. 2a) are nonseeding-competent structures. A similar result was obtained when SCL-treated and untreated samples were added to a ThT-based Aβ42 aggregation assay (fig. S6b), confirming the results obtained with the FP assay.

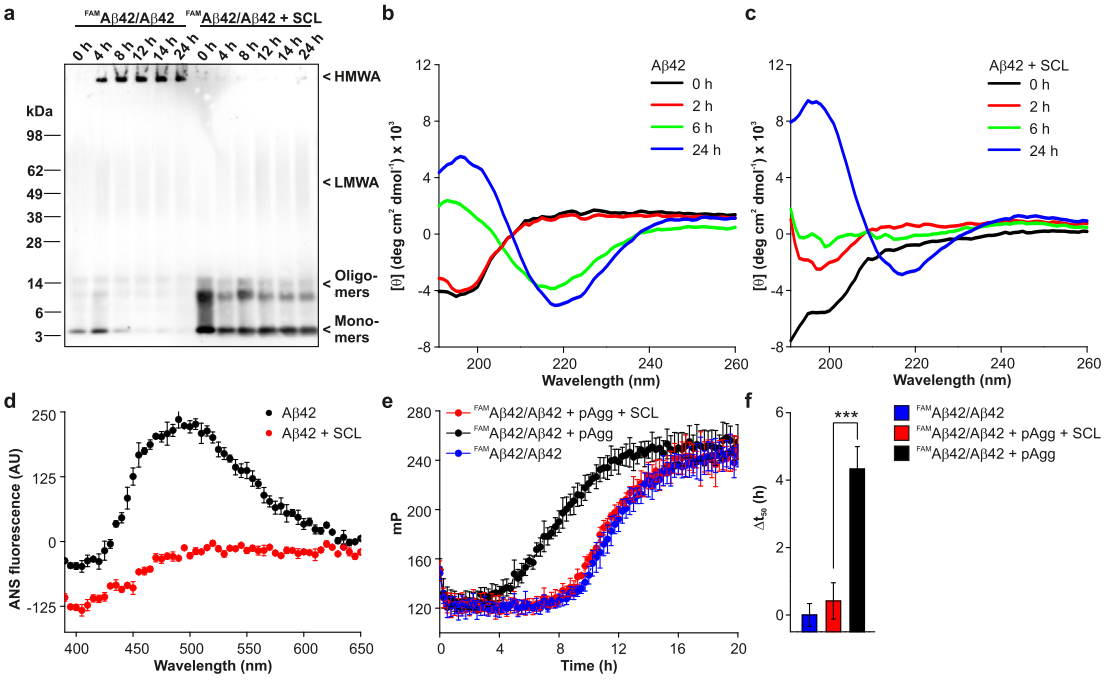

Fig. 3. SCL-stabilized Aβ42 assemblies are structures with low SDS stability and β-sheet content. (**a**) Analysis of SCL-treated (10 μM) and untreated ^{FAM}Aβ42/Aβ42 (0.1/10 μM) co-aggregation reactions by SDS-PAGE and immunoblotting using the 6E10 antibody. (**b,c**) Investigation of spontaneous Aβ42 (20 μM) aggregation in the absence (**b**) and presence (**c**) of SCL (20 μM) by CD spectroscopy. (**d**) ANS dye-binding assay. Aβ42 (20 μM) assemblies formed in the presence (20 μM) or absence of SCL show distinct ANS-binding characteristics. (**e**) Effects of SCL-treated (pAgg + SCL) and untreated (pAgg) preformed Aβ42 aggregates (100 nM monomer equivalents) on ^{FAM}Aβ42/Aβ42 (0.1/10 μM) coaggregation in FP assays. In control experiments, only SCL (0.2 μM) in the absence of preformed Aβ42 aggregates were added to FP assays. mP, milli-polarization units (**f**) Calculated Δt_{50} values from aggregation curves shown in **e.** Values are means ± SD, n = 3 (**b**, **c**, **d**) and n = 4 (**e**). Asterisks indicate significant differences as determined by the student *t*-test: *** ≤0.001.

SCL holds aggregation-prone Aβ42 peptides in a soluble state

Our studies indicate that SCL slows down Aβ42 fibrillogenesis because it interferes with very early events in the aggregation cascade. We hypothesized that SCL delays spontaneous aggregation by binding directly to unstructured Aβ42 peptides and preventing their conformational conversion into β-sheets. For addressing this question, we first carried out binding studies with nuclear magnetic resonance (NMR) techniques [35]. We treated unstructured Aβ42 monomers (50 μM) with a substoichiometric concentration of SCL (10 μM) and recorded 1H-NMR spectra after 22 h at 27 °C. We found that the resonances of the individual 1H spectra of Aβ42 peptides were sharp in compound treated samples after 22 h, while they were broadened in untreated samples (Fig. 4a–d). This indicates that the initially soluble Aβ42 peptides convert to insoluble, high-molecular-weight aggregates in untreated samples (Fig. 4a,c), while they remain soluble in SCL-treated reactions (Fig. 4b,d). The relative peak intensities from selected signals of methyl groups (Fig. 4a, ***b***) were plotted over time (Fig. 4e). We found that the relative peak intensities decrease to ~20% after 11 h in untreated samples, while they are only slightly reduced in compound-treated samples. Together these experiments indicate that SCL potently slows down Aβ42 aggregation *in vitro*, although a stable compound-peptide interaction cannot be detected in 1H NMR measurements.

In a second experiment, we recorded two-dimensional 1H and 15N spectra of treated and untreated Aβ42 samples after 24 h at 27 °C. Using this approach, we essentially confirmed that SCL treatment prevents the broadening of resonances (fig. S7a,b). Again, no major chemical shift perturbations in the 1H–15N-HSQC spectra were observed, supporting our initial results.

Finally, we performed NMR WaterLOGSY experiments to assess the interaction between SCL and Aβ42 peptides. This NMR technique is more sensitive and commonly utilized to detect interactions between polypeptides and small molecules (<1 kDa) for fragment-based lead discovery [36,37]. It allows the detection of

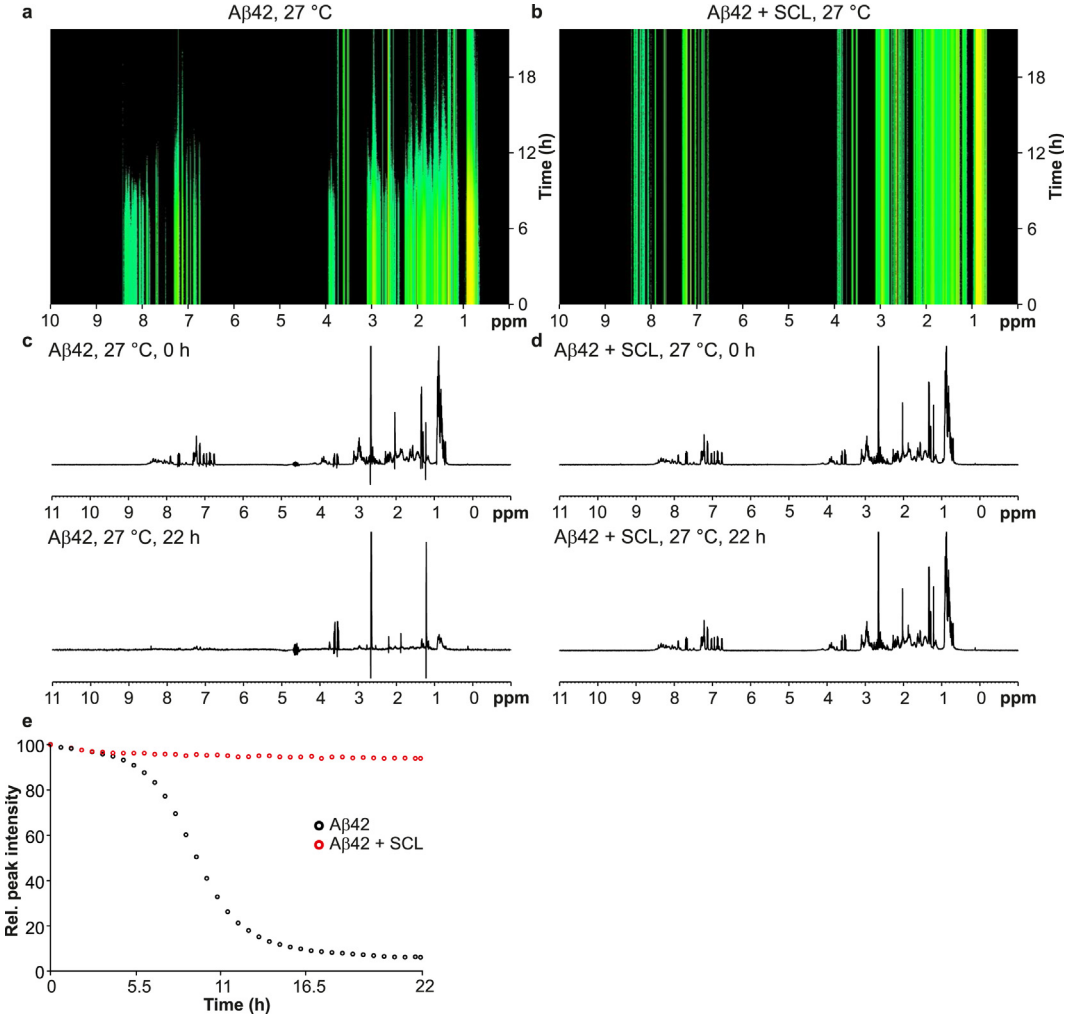

Fig. 4. SCL holds aggregation-prone Aβ42 peptides in a soluble state. (**a,b**) Time-resolved ^{1}H-NMR heat maps of untreated (**a**) and SCL-treated (10 μM) (**b**) Aβ42 (50 μM) aggregation reactions. (**c,d**) The first and last ^{1}H-NMR spectrum from the heat maps in **a** and **b** are shown; (**e**) Graphs show selected signals from the methyl group area (ppm, 0.91) of heat maps in **a** and **b.** Black circles indicate Aβ42 (50 μM) aggregation in the absence of SCL; red circles indicate SCL-treated (10 μM) Aβ42 aggregation reactions.

compound interactions without the need for 15N-labeling of backbone amides. Ligand binding to polypeptides is observed indirectly through the nuclear Overhauser effect (NOE). In these NMR experiments, the bulk water magnetization is excited and transferred during the NOESY mixing time to the bound ligand via different mechanisms [38]. The 1D spectrum of SCL with characteristic signals in the absence of Aβ42 peptides is shown in fig.S8a. The conversion of the peaks in the control experiment (SCL only) indicates that the compound does not self-aggregate in solution, which may lead to false-positive interactions in the presence of Aβ42 peptides (fig. S8b). In the NMR WaterLOGSY experiment with equal molar concentrations of SCL and Aβ42 (50 μM), no NOE was observed, while in the range of 7.5–8.8 ppm the characteristic Aβ42 signals were detectable, indicating that under these experimental conditions the Aβ42 peptides are soluble, but SCL binding cannot be detected (fig. S8c). When a 10-fold molar excess of SCL, however, was incubated with Aβ42 peptides, positive signals resulting from the compound were detectable, indicating that SCL indeed interacts with Aβ42 molecules in solution. Under these conditions, however, the typical Aβ42 signals at 7.5–8.8 ppm were undetectable (fig. S8d), indicating that the peptides form high molecular structures at high concentrations of SCL, which cannot be detected by 1D NMR WaterLOGSY experiments. Together these results indicate that SCL indeed weakly interacts with

Aβ42 peptides in solution, promoting the assembly of higher molecular weight structures.

SCL binds to Aβ42 monomers and alters their conformation

Our NMR WaterLOGSY experiments indicate that SCL weakly interacts with Aβ42 peptides, suggesting that it might slow down fibrillogenesis because it stabilizes their conformation in the nonaggregated state. For addressing this question, we performed ion mobility-mass spectrometry (IM-MS) experiments, which enable the detection of Aβ:drug interactions, as well as of transient amyloidogenic oligomers that are formed early in the aggregation cascade [39]. IM-MS separates Aβ42 peptide species based on differences in their overall size, as well as their charge [39]. It further provides an absolute rotationally averaged collision-cross section (CCS), which allows the prediction of secondary structural changes within aggregating systems, such as Aβ42 [39–41]. We analyzed Aβ42 monomers (10 μM) in the presence (40 μM) and absence of SCL after incubation for 2 h at 25 °C by IM-MS. We readily detected Aβ42 monomers with a charge state of +3 and + 4 in both compound-treated and untreated samples (Fig. 5a and b), confirming the previously reported results [42]. Interestingly, we observed a

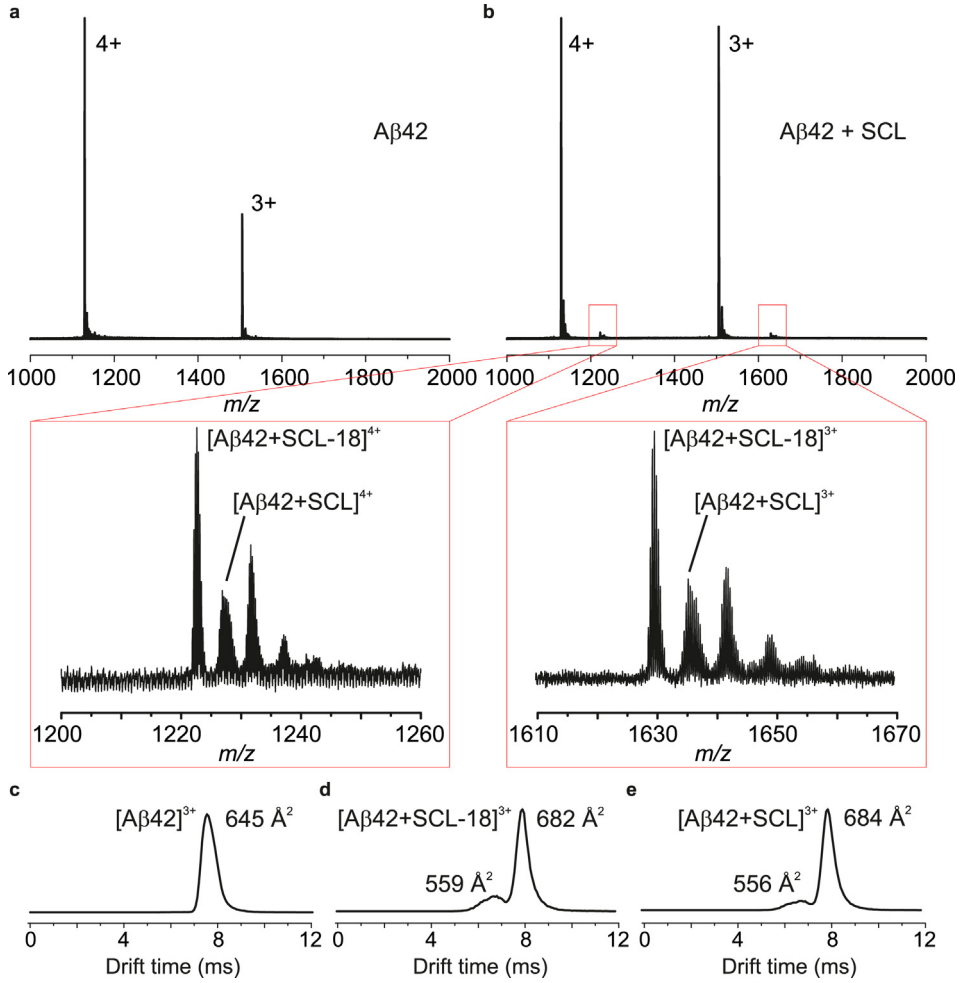

Fig. 5. SCL binding alters the conformation of Aβ42 monomers. Data were collected by ion mobility-mass spectrometry (IM-MS) using nano-electrospray ionization. (**a**) Mass spectrum of Aβ42 (10 μM) in 10 mM NH_4Ac. (**b**) Mass spectrum of Aβ42 (10 μM) in the presence of SCL (40 μM) in 10 mM NH_4Ac after 2 h at 25 °C. Lower left panel, mass spectrum of noncovalent +4 charged (z/n = +4) 1:1 Aβ42-SCL complex $[Aβ42+SCL]^{4+}$ and covalently bound SCL $[Aβ42+SCL\text{-}18]^{4+}$, magnification from **b**. Lower right panel, mass spectrum of noncovalent +3 charged (z/n = +3) 1:1 Aβ42-SCL complex $[Aβ42+SCL]^{3+}$ and covalently bound SCL $[Aβ42+SCL\text{-}18]^{3+}$, magnification from **b**. (**c**) Ion mobility spectrum of z/n = +3 charged Aβ42 $[Aβ42]^{3+}$ species with calculated cross section, (**d**) same species covalently bound to SCL $[Aβ42+SCL\text{-}18]^{3+}$ and (**e**) same species in noncovalent 1:1 complex with SCL $[Aβ42+SCL]^{3+}$.

relative increase of 3+ monomers in SCL-treated samples, suggesting that SCL influences this Aβ42 monomer population by a dynamic assembly-disassembly process. This is further supported by additional changes at $m/z = 1625-1655$ and $m/z = 1220-1240$ in compound-treated samples (Fig. 5b), indicating that SCL binds either covalently (*e.g.*, $[A\beta42+SCL\text{-}18]^{3+/4+}$, due to water loss) or noncovalently (*e.g.* $[A\beta42+SCL]^{3+/4+}$) to Aβ42 monomers. Strikingly, IM-MS experiments further showed that these compound interactions significantly alter the conformation of Aβ42 peptides. Untreated samples showed a narrow, single population of Aβ42 monomers with an averaged overall size of 645 $Å^2$, whereas the compound-treated samples showed, independent of the binding mode (*e.g.* covalent $[A\beta42+SCL\text{-}18]^{3+/4+}$ or noncovalent $[A\beta42+SCL]^{3+/4+}$), an appearance of a second Aβ42 monomer population. The major conformation of the SCL-bound species $[A\beta42+SCL]^{3+}$ (684 $Å^2$) showed a slight increase in size compared to the free Aβ42 monomers $[A\beta42]^{3+}$ (645 $Å^2$). This is expected due to ligand binding. However, a second additional conformation appeared upon SCL binding to the Aβ42-monomer, which adopts a significantly more compact structure (556 $Å^2$) than the free monomer. Such compact, unstructured conformations of Aβ42 peptides were previously shown to be less aggregation-prone [43,44] and to have a low β-sheet content [45,46]. Together these studies suggest that SCL binding leads to conformational compaction at least in a small fraction of Aβ42 monomers, which may influence their conversion rate into aggregation-competent β-sheet-rich fibrils.

Neuroblastoma cells take up small SCL-stabilized Aβ42 assemblies less efficiently than larger fibrillar aggregates

Recent studies indicate that β-sheet-rich, fibrillar Aβ42 aggregates are more easily taken up into mammalian cells than unstructured monomers [47], suggesting that small SCL-stabilized Aβ42 assemblies might enter cells less efficiently than larger

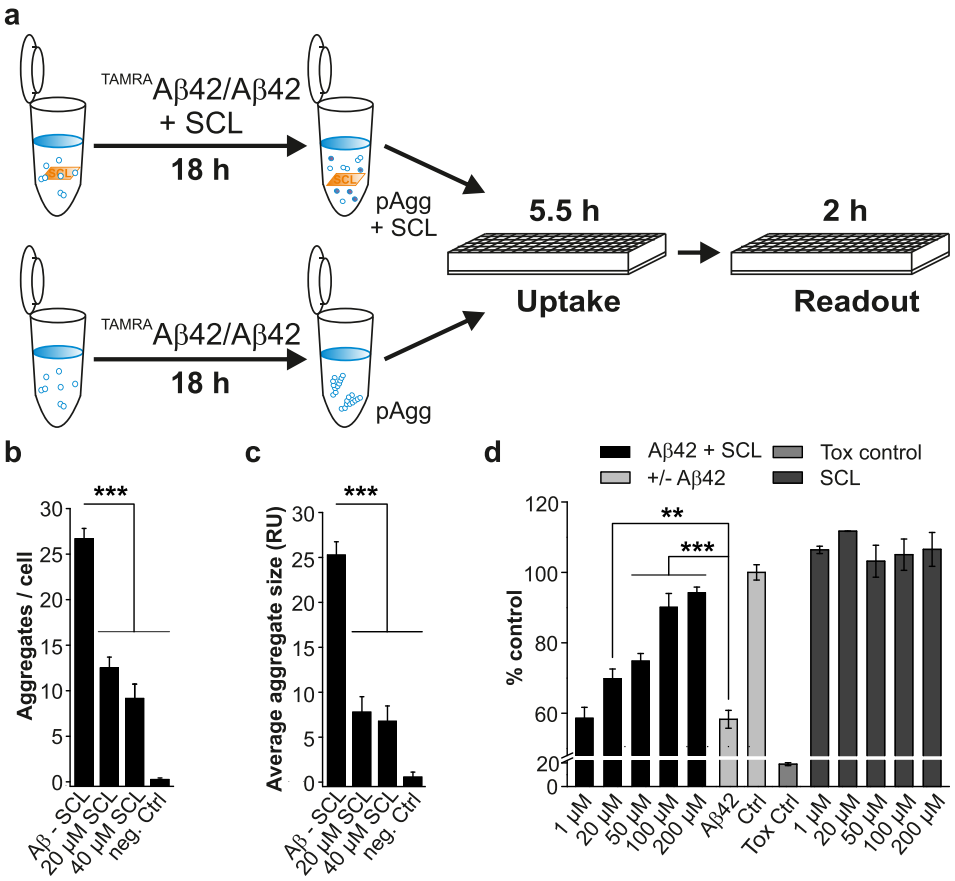

Fig. 6. SCL treatment leads to reduced cellular Aβ42 aggregate uptake and toxicity. (**a**) Schematic representation of cellular aggregate uptake experiments. pAGG, pre aggregated material. (**b, c**) Quantification of number (**b**) and size (**c**) of aggregates (fluorescent foci) in mammalian cells. (**d**) Quantification of toxicity of SCL-treated and untreated Aβ42 aggregation reactions with MTT assays. Aggregation reactions were added after incubation for 24 h at 37 °C to PC12 cells. Values are means ± SD, n = 4 (**d**), 8 (**b**, **c**); Asterisks indicate significant differences as determined by the student *t*-test: * ≤ 0.05, ** ≤ 0.01, *** ≤ 0.001.

structures. To address this question, we first treated a mix of TAMRA-labeled (1 μM) and unlabeled Aβ42 peptides (20 μM) with SCL (20 and 40 μM) and incubated this reaction for 18 h at 37 °C to obtain fluorescently labeled nonfibrillar SCL-stabilized Aβ42 assemblies **(Fig. 6a)**. We confirmed by AFM that the fibrillar ^{TAMRA}Aβ42/Aβ42 co-aggregates are morphologically very similar to Aβ42 fibrils and that the treatment of samples with SCL decreases the spontaneous formation of large fibrillar structures *in vitro* (fig. S9). Next, SH-EP neuroblastoma cells were incubated for 5.5 h with the SCL-treated and untreated fluorescently labeled Aβ42 aggregate species. Incubation for ~5 h was previously shown to be sufficient for the uptake of a large fraction of fibrillar Aβ42 aggregates into SH-EP cells [47]. After extensive washing to remove extracellular aggregates, cells were transferred into a new microtiter plate for image analysis. After further incubation for 2 h at 37 °C, the number of TAMRA-labeled Aβ42 puncta in cells was quantified by high-content fluorescence imaging. Strikingly, we detected significantly lower numbers of TAMRA-positive puncta when cells were treated with small SCL-stabilized structures rather than untreated Aβ42 aggregates (Fig. 6b), indicating that untreated fibrillar Aβ42 aggregates are internalized much more efficiently into mammalian cells than small SCL-stabilized Aβ42 oligomers (fig. S9). This result was confirmed when the size of intracellular TAMRA-positive puncta was quantified by automated fluorescence microscopy (Fig. 6c).

SCL treatment decreases Aβ42 aggregate toxicity in PC12 cells

Finally, we carried out standardized colorimetric 3-(4,5-dimethylthiazol-2-yl)-2,5-diphenyltetrazolium bromide (MTT) reduction assays [48] with PC12 cells to assess the toxicity of SCL-treated and untreated Aβ42 aggregation reactions. We first incubated Aβ42 monomers for 22 h at 37 °C with different concentrations of SCL (1−200 μM). Then, the Aβ42 aggregation reactions were added to PC12 cells, and cultures were incubated for 72 h at 37 °C. Finally, MTT reduction was quantified in PC12 cells using the established colorimetric assay [48]. We found that β-sheet-rich fibrillar Aβ42 aggregates (untreated samples) cause a pronounced inhibition of MTT reduction (~40%, Fig. 6d), confirming previously reported observations that such structures are toxic and decrease the metabolic activity of PC12 cells [23]. However, inhibition of MTT reduction was diminished in a concentration-dependent manner when SCL-treated samples were analyzed, indicating that small compound-stabilized oligomers (Fig. 2a,d) are less toxic in MTT assays than large fibrillar, β-sheet-rich Aβ42 aggregates. No inhibition of MTT reduction was observed when respective concentrations of SCL were added to PC12 cells in the absence of Aβ42 peptides (Fig. 6d).

Discussion

The formation of large pathogenic, β-sheet-rich Aβ42 aggregates from natively unstructured monomers is a complex multistep process involving the assembly of various potentially proteotoxic aggregate species, such as small oligomers, protofibrils, or fibrils [6,9]. This suggests that an effective therapeutic strategy with small molecules should interfere with very early steps in the aggregation cascade before such toxic structures are formed. Compounds may be found that maintain Aβ42 monomers in their native, unstructured state and thus hinder their conversion into β-sheet-rich fibrillar aggregate species. However, due to the fact that Aβ42 monomers in aqueous solutions are intrinsically unfolded structures, the stabilization of their native state with small-molecule binders is challenging [49].

In this study, we have identified the small molecule sclerotiorin (SCL) that potently slows down both seeded and nonseeded Aβ42 fibrillogenesis in cell-free assays (Fig. 1a−f). SCL consists of a highly oxygenated aromatic ring system and a nine-carbon aliphatic diene side chain [25], suggesting that its amphipathic properties are critical for its effects on Aβ42 aggregation. Amphipathic small molecules and peptides have previously been identified as enhancers and inhibitors of Aβ42 and tau aggregation [50−52]. Their mechanisms of action, however, remain largely unclear. Here, we provide experimental evidence that at least a small fraction of unstructured Aβ42 peptides directly binds to the chemical compound SCL (Fig. 5b *and* fig S8a-d), suggesting that a weak compound interaction is sufficient to slow down fibrillogenesis. Previous investigations indicate that an interaction between the small molecule 10058-F4 and unstructured MyC peptides prevents their spontaneous assembly into β-sheet-rich aggregates [53]. Furthermore, a large number of reports indicate that the potent aggregation inhibitor EGCG [23] binds weakly to soluble, unstructured aggregation-prone polypeptides, such as Aβ and α-synuclein, and decreases their propensity to self-assemble into stable amyloid structures [54,55].

Our data suggest that the interaction of SCL with only a small fraction of aggregation-prone Aβ42 molecules in a large population of unstructured Aβ42 conformers is sufficient to efficiently slow down the overall aggregate formation process (Fig. 1b−f). The spontaneous formation of stable, aggregation-competent, β-sheet-rich Aβ42 structures in a population of unstructured molecules is a rare and energetically unfavorable event [11,56]. Thus, compounds that

interfere with the process of primary nucleation, which occurs very early in the aggregation cascade, should be active at substoichiometric concentrations *in vitro* and *in vivo*.

We gained experimental evidence that SCL weakly interacts with aggregation-prone Aβ42 peptides in solution (fig. S8a-d). We suggest that it may directly associate with the central or the C-terminal hydrophobic regions in Aβ42 peptides [57], which facilitate β-sheet formation and promote the intermolecular association of monomers [58]. This may involve the hydrophobic diene side chain in the small molecule (Fig. 1a). However, the oxygenated bicyclic ring system in SCL may also be critical for targeting aggregation-prone Aβ42 peptides. It may form covalent bonds with polar amino acids in the Aβ42 peptide, such as Lys 16 or Lys28 that are important for the formation of a stable, aggregation-competent β-hairpin structure [58]. Our IM-MS experiments confirm this view and indicate that at least a small fraction of Aβ42 monomers covalently interact with SCL (Fig. 5a–c). Preliminary investigations of the SCL:Aβ42 complex with higher-energy C-trap dissociation experiments (unpublished results) also support this hypothesis. However, further studies are necessary to substantiate these initial results.

We suggest that the SCL interaction affects the conformational space of aggregation-prone, disordered Aβ42 peptides, and stabilizes the formation of aggregation-incompetent, small oligomers prior to the formation of fibrillar aggregates [49]. Recent biochemical and biophysical investigations support our hypothesis that aliphatic structures can directly target aggregation-prone Aβ40 peptides and prevent their assembly into amyloid aggregates *in vitro* [59]. Our studies indicate that SCL, even at very low concentrations, converts unstructured Aβ42 monomers into small, seeding-incompetent, spherical oligomers with a low aggregation-propensity (Figs. 2 and 3). Similar structures have previously been obtained when aggregation-prone unstructured α-synuclein and Aβ42 polypeptides were treated with the polyphenol EGCG [23]. However, our investigations revealed that the SCL-stabilized oligomers readily dissociate into monomers upon SDS treatment (Fig. 3a), while this is not the case in the presence of EGCG [23]. This demonstrates that the SCL- and EGCG-generated oligomers are distinct in terms of their biochemical properties. We suggest that EGCG stabilizes Aβ42 oligomers because it cross-links unstructured polypeptides [60]. However, such a mechanism of action most likely is not operational with SCL. Our MS-based investigations (Fig. 5b) indicate that the Aβ42 peptides are not cross-linked upon SCL treatment. Under the experimental conditions used, only stable interactions between Aβ42 monomers and SCL molecules were readily observed. We suggest that SCL promotes the intermolecular association of monomers due to its amphipathic properties [25], leading to the formation of relatively small, unstable Aβ42 oligomers (Fig. 2a). A similar mechanism of action was previously described for the small-molecule aggregation inhibitor FN075 that triggers both CsgA and α-synuclein oligomer formation [61].

Experimental evidence has been provided that a large number of fibrillar but also nonfibrillar aggregate assemblies with β-sheet-rich domains cause dysfunction and toxicity in cell-based assays [23,62,63]. This suggests that stable β-sheets in aggregate assemblies are important molecular determinants of cellular toxicity. Our investigations with PC12 cells and SCL-treated and untreated aggregation reactions support these observations. We found that in comparison to untreated reactions, inhibition of MTT reduction was significantly decreased in SCL-treated samples (Fig. 6d), suggesting that β-sheet-rich fibrillar rather than unstructured nonfibrillar Aβ42 assemblies cause dysfunction and toxicity in cells. This result is also supported by our observations that fibrillar Aβ42 assemblies are taken up into cells much more efficiently than nonfibrillar structures (Fig. 6b and c). Recent investigations indicate that intraneuronal Aβ structures cause dysfunction and drive pathogenesis in AD [64], suggesting that the uptake of Aβ aggregates is a prerequisite for the induction of toxicity in PC12 cells. Our results agree with previous observations that fibrillar Aβ42 assemblies are internalized into neuronal cells much more efficiently than nonfibrillar structures [47]. Furthermore, they substantiate investigations indicating that β-sheet-rich Aβ assemblies expose unique hydrophobic surfaces and efficiently disrupt membranes in cell-free assays [63]. Finally, they confirm the hypothesis that small, seeding-competent fibrillar amyloid assemblies are disease-relevant species with high cellular toxicity [8,23,65–67].

Overall, our study suggests that compounds targeting and stabilizing small unstructured Aβ42 oligomers with low β-sheet content could be useful for therapy development. Stabilizing of folded transthyretin (TTR) tetramers with the small molecule tafamidis has been shown to be effective for the treatment of familial amyloid polyneuropathy (FAP), a disease associated with the misfolding and aggregation of the protein TTR [19]. We hypothesize that drug combinations targeting different individual microscopic steps in the amyloid aggregation cascade may be an effective therapeutic strategy for the treatment of AD. Besides compounds that stabilize unstructured Aβ42 oligomers and thereby slow down primary and secondary nucleation steps [68], compounds that target and disrupt more mature β-sheet-rich amyloid structures may also

be of high value. A small molecule with such activity has recently been described to successfully decrease plaque pathology, aggregate-related inflammatory expression changes, and disease symptoms in a transgenic AD model [21]. On the basis of the mechanistic studies presented here, we conclude that SCL or compounds with a similar mode of action may have considerable potential as drug candidates for the treatment of AD. Previously, related azaphilone compounds from fungi have been described as modulators of tau aggregation *in vitro* [52].

Materials and Methods

Aβ42 peptide stock solutions

Synthetic Aβ1-42 (Aβ42) was purchased from Bachem (Bubendorf, Switzerland, #H-1368) and dissolved in 1,1,1,3,3,3-Hexafluoro-2-propanol (HFIP) to 5 mg/ml, vortexed for 1 min and sonicated for 10 min (ultrasonic bath, SONOREX DIGITEC, Bandelin, Berlin Germany) at 4 °C. The solution was incubated 3 times at 22 °C for 1 h, vortexed for 1 min, sonicated for 1 min, stored for 67 h at 22 °C, aliquoted and lyophilized (RVC 2–25 CDplus, Christ, Osterode am Harz, Germany). Monomeric Aβ42 solutions were prepared from the aliquots by dissolving the peptide in 10 mM NaOH to 200 μM, followed by 1 min vortexing and 5 min sonication. Aggregation reactions were started by mixing 200 μM Aβ42 peptide stock solutions with low salt buffer (LSB: 10 mM KH_2PO_4, 10 mM K_2HPO_4, 10 mM NaCl, pH 7.4) to obtain final peptide concentrations. All concentrations of fibrillar Aβ42 species refer to the equivalent concentration of Aβ42 monomers.

Fibrillar Aβ42 seeds

Synthetic Aβ1-42 (Aβ42) peptides produced by the laboratory of Dr. Volkmer-Engert (Institute for Medical Immunology, Charité - Universitätsmedizin Berlin, Germany) were dissolved in HFIP, vortexed for 1 min followed by incubation for 1 h at 20 °C (four times) and sonication (ultrasonic bath, SONOREX DIGITEC, Bandelin, Berlin Germany) for 10 min. After additional incubation of 16 h at 20 °C and 30 min sonication, the solution was aliquoted, frozen in liquid nitrogen, lyophilized with a vacuum concentrator RVC 2–25 CDplus (Christ, Osterode am Harz, Germany), and stored at 20°C. For the preparation of fibrillar assemblies (FAs), aliquots were dissolved in 100 mM NaOH to 10 mg/ml; vortexed for 1 min, sonicated for 5 min, dissolved with a low salt buffer to 200 μM and incubated for 6 h at 37 °C at 300 rpm. Aliquots were stored at 80°C.

Fluorescence polarization-based Aβ42 aggregation assay

Carboxyfluorescein labeled β-amyloid [1–42] peptides (Anaspec, Fremont, USA, #AS-23525) were dissolved in 1 mM NaOH to 50 μM and stored as a stock solution. 0.1 μM of this tracer together with 10 μM Aβ42 monomers in LSB were combined with 40 nM Aβ42 FAs (seeds) and test compounds (1 μM). The aggregation mixtures were replenished with LSB to a total volume of 40 μl. The fluorescence polarization measurements were carried out for a minimum of 16 h with a single measurement every 15 min at 37 °C in a plate reader (Infinite M1000/Infinite M1000 PRO, Tecan, Männedorf, Switzerland) at an excitation wavelength of 470 ± 5 nm and an emission wavelength of 528 ± 20 nm in 384-well plates with 5 s shaking before each reading. Values are means of five technical replicates. Polarization values are expressed as dimensionless mP values, calculated by the plate-reader software i-control (Tecan, Männedorf, Switzerland).

Preparation of Aβ seeds from mouse brains

Frozen tissue was weighed and homogenized in a 5-fold excess (w/v) of ice-cold 50 mM Tris-HCl pH 7.5, 150 mM NaCl, 0.1% SDS, 0.5% Sodium deoxycholate, 1% Triton X-100, 0.25 U/μl Benzonase and a complete protease inhibitor cocktail using a schuett homgen^{plus} (schuett-biotec GmbH, Goettingen, Germany) semi-automatic homogenizer (700 rpm). The homogenate was centrifuged for 20 min at 1500×*g* at 4 °C to remove cell debris. The supernatant was transferred to a new tube, and the total protein concentration was determined with the Pierce BCA assay (ThermoFisher Scientific/Life Technologies GmbH, Darmstadt, Germany) using BSA as a standard. Seeding-competent Aβ aggregate species were enriched from mouse brain homogenates (prepared from 0.25 mg brain tissue of APPPS1 transgenic mice) through immunoprecipitation with magnetic protein G beads (Pierce™ Protein G Magnetic Beads, ThermoFisher Scientific/Life Technologies GmbH, Darmstadt, Germany) coated with 6E10 antibody. Antibody bound beads were incubated with homogenate at room temperature for 30 min. Beads were then washed three times in LSB before being subjected to sonification for 30 s (Model 120 Sonic Dismembrator, Fisher Scientific GmbH, Schwerte, Germany). Aβ aggregate species (10 μl) released from beads by sonication were used as seeding-competent material in FP assays.

Biochemical characterization of Aβ42 assemblies in FP assays

Co-aggregation of Aβ42 (10 μM) and ^{FAM}Aβ42 (0.05 μM) in the presence (2 or 10 μM) and absence of chemical compounds was monitored in a time-dependent manner by quantification of FP. The impact of seeds on spontaneous ^{FAM}Aβ42/Aβ42 co-aggregation was assessed by the addition of preformed Aβ42 fibrils (100 nM) to reactions. After 4, 8, 12, 14, and 24 h, the FP measurements were interrupted, and samples were taken from the microtiter plate and stored on ice. Finally, compound-treated and untreated ^{FAM}Aβ42/Aβ42 coaggregates were analyzed by SDS- or BN-PAGE followed by immunoblotting. In addition, ^{FAM}Aβ42/Aβ42 aggregate species were assessed by AFM, EM, dot blot, or filter assays.

Compounds

Sclerotiorin (SCL, # 89460, Cayman Chemicals, Ann Arbor, USA, $\geq$ 98% or # AG-CN2-0054, AdipoGen Life Services, San Diego, USA, SCL $\geq$ 97%), Epigallocatechin gallate (EGCG, # 93894, Sigma-Aldrich/Merck (Germany, $\geq$ 95%), Wedelolactone (WED, #W4016, Sigma-Aldrich/Merck (Germany, $\geq$ 98%), a-apo-Oxytetracycline (a-OXY, # A1220000, Sigma-Aldrich (Germany, $\geq$ 98%).

Antibodies

Commercially available antibodies applied in this study are anti-β-amyloid 1−16 antibody (clone 6E10, Biolegend, USA) and anti-mouse IgG and peroxidase-conjugated IgGs for immunoblots (Sigma-Aldrich/Merck, Munich, Germany). The fibril-specific monoclonal anti-β-amyloid antibody 352 [21] is commercially available at Synaptic Systems GmbH (Goettingen, Germany).

Thioflavin T assay

The aggregation of HFIP treated Aβ42 peptides (25 μM) was monitored over time with Thioflavin T (ThT, 25 μM) in the presence or absence of chemical compounds. For stimulating aggregation preformed short Aβ42 fibrils (250 nM) were added as seeds to reactions. ThT fluorescence was measured in LSB over 16 h at 37 °C. ThT fluorescence was recorded using a plate reader (Infinite M200, Tecan, Männedorf, Switzerland) with 15 min reading intervals and 5 s shaking before each read using an excitation wavelength of 420 ± 9 nm and an emission wavelength of 485 ± 20 nm.

Seeding activity of SCL-treated and untreated Aβ42 aggregation reactions

Aβ42 monomers (10 μM) were incubated for 18 h at 37 °C in the presence and absence of SCL (10 μM). Then, the generated Aβ42 assemblies (250 or 100 nM) were added as seeds to ThT- (25 μM Aβ42, 25 μM ThT) and FP-based (10 μM Aβ42, 0.05 μM tracer) aggregation assays, respectively. In the control experiments, respective SCL concentrations (250 or 100 nM) were added to ThT and FP reactions in the absence of preformed Aβ42 assemblies.

ANS assay

Aβ42 peptides (20 μM) were incubated without or with 20 μM SCL for 24 h. Then, 8-Anilino-1-naphthalene sulfonic acid ammonium salt (ANS, 100 μM; # A1028 Sigma-Aldrich, Germany) was added to reactions, and fluorescence spectra were measured with an excitation wavelength of 350 nm ± 10 nm and an emission between 380 nm ± 20 nm and 650 nm ± 20 nm using a plate reader (Infinite M200, Tecan, Männedorf, Switzerland).

Analysis of Aβ42 assemblies by SDS- and BN-PAGE followed by immunoblotting

Samples from Aβ42 aggregation reactions (4.5 μl, 10 μM) were mixed with 2.5 μl of NuPAGE LDS sample buffer (ThermoFisher Scientific, Germany), 2.9 μl LSB buffer and 0.1 μl 5 M DTT and boiled for 5 min at 96 °C before they were loaded onto a NuPAGE Bis-Tris 4−12% gel (ThermoFisher Scientific, Germany). SDS-PAGE analysis was performed without DTT and heated denaturing. For the investigation of Aβ42 aggregates under nondenaturing conditions Novex Bis-Tris 4−16% gels (ThermoFisher Scientific, Germany) were used. 4.5 μl of Aβ42 samples (10 μM), 2.5 μl of NativePAGE 4 × Sample Buffer (ThermoFisher Scientific, Germany) and 3 μl LSB buffer were loaded in each well. Separation of Aβ42 assemblies on SDS or native gels was performed according to standard protocols. Aβ42 peptides retained on membranes were visualized by immunoblotting using the 6E10 antibody.

Atomic force microscopy

20 μl of spontaneously formed Aβ42 aggregates (10 μM) were added onto a freshly cleaved sheet mica (Nanoworld, Switzerland), which was glued on a microscope slide and incubated for 10 min. The solution was removed with a lint-free cloth and washed 4 × with Milli-Q H_2O. The samples were dried, and AFM images were recorded on a Nanowizard II/Zeiss Axiovert setup (JPK, Germany) using an intermittent contact mode and FEBS cantilevers (Veeco, USA).

Dot blot assay

Samples with Aβ42 monomers or aggregates (50 and 100 ng) were filtered through nitrocellulose membranes (0.45 μm; GE Healthcare Life Sciences, Germany). Membranes were then blocked for 30 min with 3% skim milk in PBS containing 0.05% Tween. After washing, membranes were incubated with the sequence-specific anti-Aβ antibody 6E10 (dissolved 1:1000 in PBS with 3% skim milk containing 0.05% Tween) overnight, washed with PBS (0.05% Tween) and incubated with a horseradish peroxidase-conjugated secondary antibody (Promega, Germany) for 1 h. Membranes were developed with ChemiGlow West Chemiluminescence Substrate (Alpha Innotech, USA), and chemiluminescence was measured with FujiFilm LAS-3000 (Fuji Photo Film (Europe) GmbH, Germany. Dot blots were quantified using the AIDA Image Analyzer software (Raytest, Germany).

Filter retardation assay

In denaturing filter retardation assays (dFRAs), Aβ42 aggregates (200 or 400 ng) were monitored after adding an equal volume of 4% sodium dodecyl sulfate (SDS) and 100 mM dithiothreitol (DTT) to reactions. Samples were boiled at 98 °C for 5 min before filtering them through a cellulose acetate membrane with a pore size of ~0.2 μm (GE Healthcare Life Sciences, Germany). For analysis of Aβ42 aggregates under nondenaturing conditions in a native filter retardation assay (nFRA), Aβ42 aggregation reactions (200 or 400 ng) were filtered through a cellulose acetate membrane without SDS and DTT treatment. Membranes were blocked for 30 min with 3% skim milk in PBS containing 0.05% Tween and aggregates

retained on filter membrane were quantified by immunoblotting.

MTT assay

For assessing the toxicity of Aβ42 assemblies formed in the presence (1, 20, 50, 100, 200 μM) or absence of SCL, HFIP treated Aβ42 peptides were dissolved to 200 μM in 10 mM NaOH and immediately diluted with SCL in LSB to 15 μM. Then, the samples were incubated for 24 h at 37 °C and 300 rpm in an Eppendorf shaker. 10 μl of these aggregation reactions were mixed with 90 μl medium and added to PC12 cells (20,000 cells/well in a 96 well microtiter plate; Greiner Bio-ONE, no. 655,180, Germany). Cells with SCL-treated and untreated aggregation reactions were incubated for 72 h at 37 °C. MTT reagent (15 μl, Promega GmbH, CellTiter 96® Nonradioactive Cell Proliferation Assay, Mannheim, Germany) was added to each well. Then, after an incubation of 4 h the color reaction was quenched by adding stop solution (100 μl). Samples were incubated for 1 h. The absorption was measured in a plate reader (Infinite M200, Tecan, Männedorf, Switzerland). Values were calculated as % DMSO control (mean ± SD, n = 3–5 technical replicates; all experiments were repeated 3 times with very similar results). As a positive control, cells were treated with 50 μM cycloheximide. Also, corresponding SCL concentrations without Aβ42 aggregates were analyzed.

Uptake of Aβ42 aggregates into mammalian cells

HFIP treated Aβ42 peptides were dissolved to 200 μM in 10 mM NaOH and immediately diluted with TAMRA-labelled Aβ42 peptides (^{TAMRA}Aβ42, 50 mM in 10 mM NaOH) in LSB to obtain a concentration of 20 μM. The final concentration of TAMRA-labelled Aβ42 peptides in this solution was 5%. Then, the mixture of ^{TAMRA}Aβ42/Aβ42 peptides was aggregated in the presence (20, 40 μM) and absence of SCL for 18 h. Finally, the generated ^{TAMRA}Aβ42/Aβ42 coassemblies were sonicated (Model 120 Sonic Dismembrator, Fisher Scientific GmbH, Schwerte, Germany) 6-times for 10 s on ice.

Preformed compound-treated and untreated ^{TAMRA}Aβ42/Aβ42 co-assemblies (600 nM) were added to SH-EP cells (900,000 cells/well, in a 6-well plate cultured for 1 day in DMEM, 31885-049, Life Technologies, US) and incubated for 5.5 h. Then, the cells were washed with 2 ml PBS, trypsinized (0.5 ml), centrifuged, and resuspended in 2 ml cell medium. The cell number was adjusted (450,000 cells per ml), and 80 μl of the suspension was incubated for 2 h with 80 μl cell medium in a 96-well microtiter plate. The cell nuclei were stained with Hoechst 33342 (1:2500 dilution of bis-Benzimide H 33342 trihydrochloride, Sigma-Aldrich/Merck, Munich, Germany). Finally, cells were fixed with a final concentration of 2% formaldehyde and washed 2 times with PDS (200 μl). The number of cells, as well as the number and sizes of ^{TAMRA}Aβ42/Aβ42 co-aggregates in cells, were quantified using the Cellomics technology (mean ± SD, n = 10–15 technical replicates; all experiments were independently repeated 2 times with very similar results).

Solution NMR

Samples were prepared by mixing 40 μl of Aβ42 peptides in 10 mM NaOH with 530 μl LS buffer. Subsequently, 30 μl DMSO-d_6 were added, either pure DMSO-d_6 or a stock solution of SCL in DMSO-d_6 (1 mM or 200 μM to yield concentrations of 10 or 50 μM, respectively). The solutions were then transferred into a 5 mm sample tube and inserted into the magnet. After mixing the solutions, the NMR experiments were started after 5 or 10 min. The resulting 5% of DMSO-d_6 were used for the lock during the experiments. Experiments were performed at 280 or 300 K on an AV–III–600 NMR-spectrometer (600 MHz ^{1}H frequency, Bruker Biospin, Karlsruhe, Germany) equipped with a TCI cryoprobe with one-axis self-shielded gradients. Temperatures were calibrated using d_4-methanol. Topspin 3.2 was used to control the spectrometer. One-dimensional NMR experiments were performed using 3-9-19 WATERGATE [69] water suppression implemented in an excitation sculpting sequence [70] and recording 4096 complex points (acquisition time 409.6 msec), a relaxation delay of 1.3 s and 128 scans. Decay curves were recorded using the same pulse sequence in a pseudo-2D experiment with 350 FIDs, covering a time of 22 h. Two-dimensional, ^{1}H,^{15}N-correlations were performed either as HSQC experiments [71] or as SOFAST-HMQC [72] experiments. 512(^{1}H)*128(^{15}N) complex points were acquired, with $t_{H,max}$ = 51.2 ms, $t_{N,max}$ = 64 ms and 64 scans. WaterLOGSY experiments were performed using reported information from the literature [73] and recording 4096 complex points (acquisition time 409.6 msec), a relaxation delay of 1.3 s, an exchange delay of 2.3 s, a trim pulse of 30 msec and 128 scans. NMR data were processed, and spectra viewed using topspin 3.2 (Bruker Biospin, Karlsruhe, Germany). The resonance assignment of the ^{1}H,^{15}N-correlation was transferred from Roche et al. [74].

IM-MS measurements

Linear drift tube (DT) IM-MS measurements were performed on a modified Synapt G2-S HDMS (Waters Corporation, Manchester, UK) described in detail elsewhere [75]. Prior to IM-MS measurements the freeze-dried aliquot of the Aβ42 peptides was diluted to obtain a 10 μM concentrated solution either in a) 10 mM ammonium acetate buffer +0.1% (v/v) DMSO or in b) 10 mM ammonium acetate buffer + 0.1% (v/v) DMSO containing 40 μM SCL. For nano-electrospray ionization (nano-ESI), typically, 5 μl of the sample was loaded and electrosprayed by applying 1.1 kV capillary voltage. Further parameters were: 30 V sampling cone voltage, 30 V source offset voltage, 30 °C source temperature, 0 V trap CE, 0 V transfer CE, 2 ml/min trap gas flow. Ion mobility parameters were: 2.2 Torr helium IMS gas, 27 °C IMS temperature, −5.0 V trap DC entrance voltage, 6.0 V trap DC bias voltage, −5.0 V trap DC voltage, 1.0 V trap DC exit voltage, −25.0 V IMS DC entrance voltage, 70–110 V helium cell DC voltage, −40.0 V helium exit voltage, 70–100 V IMS bias voltage, 0 V IMS DC exit voltage, 5.0 V transfer DC entrance voltage, 15.0 V transfer DC exit voltage, 150 m/s trap wave velocity, 2.0 V trap wave height voltage, 150 m/s transfer wave

velocity, 2.0 V transfer wave height voltage. IM-MS spectra were recorded in the positive ion mode, and drift times were converted to rotationally-averaged collision cross-sections (CCS) using the Mason-Schamp equation [76].

General

We thank A. Boeddrich for her general support in preparing the manuscript and M. Peters for expert discussions.

Funding

This study received funding from the GO-Bio initiative of the German Federal Ministry for Education and Research (BMBF), grant no. BMBF 0313881; from the ERA-NET NEURON initiative "ABETA ID" of the BMBF, grant no. BMBF 01W1301; from the Collaborative Research Grant in the framework of the Berlin Institute of Health (BIH), grant no. CRG 1.1.2.a.3; from the Helmholtz Validation Fund of the Helmholtz Association, grant no. HVF-0013; and from the Stiftung Charité / Private Excellence Initiative Johanna Quandt, Germany - all to E.E.W.

Data availability

All data generated and analyzed in this study are available with the paper online.

Author contributions

T.W., N.G., W.H, C.M., L.D., A.B., L.B., N.N. and P.S. performed experiments; S.S., K.P., C.H. and E.E.W. edited the manuscript; E.E.W. and T.W. designed the study and prepared the manuscript. E.E.W. supervised the project.

Conflict of interest statement

None.

Appendix A. Supplementary data

Supplementary data to this article can be found online at https://doi.org/10.1016/j.jmb.2020.01.033.

Received 25 September 2019;
Received in revised form 14 January 2020;
Accepted 28 January 2020
Available online 13 February 2020

Keywords:
biochemistry;
protein aggregation;
small molecules;
NMR WaterLOGSY;
mass spectrometry

[†]Both authors contributed equally.

References

[1] C.L. Masters, R. Bateman, K. Blennow, C.C. Rowe, R.A. Sperling, J.L. Cummings, Alzheimer's disease, Nat Rev Dis Primers 1 (2015) 15056.
[2] J. Wang, B.J. Gu, C.L. Masters, Y.J. Wang, A systemic view of Alzheimer disease - insights from amyloid-beta metabolism beyond the brain, Nat Rev Neurol. 13 (2017) 612–623.
[3] J.D. Harper, P.T. Lansbury Jr., Models of amyloid seeding in Alzheimer's disease and scrapie: mechanistic truths and physiological consequences of the time-dependent solubility of amyloid proteins, Annu Rev Biochem. 66 (1997) 385–407.
[4] M. Jucker, L.C. Walker, Self-propagation of pathogenic protein aggregates in neurodegenerative diseases, Nature 501 (2013) 45–51.
[5] C. Haass, D.J. Selkoe, Soluble protein oligomers in neurodegeneration: lessons from the Alzheimer's amyloid beta-peptide, Nat Rev Mol Cell Biol. 8 (2007) 101–112.
[6] I. Benilova, E. Karran, B. De Strooper, The toxic Abeta oligomer and Alzheimer's disease: an emperor in need of clothes, Nat Neurosci. 15 (2012) 349–357.
[7] M. Fandrich, Oligomeric intermediates in amyloid formation: structure determination and mechanisms of toxicity, J Mol Biol. 421 (2012) 427–440.
[8] R. Gallardo, M. Ramakers, F. De Smet, F. Claes, L. Khodaparast, L. Khodaparast, J.R. Couceiro, T. Langenberg, M. Siemons, S. Nystrom, L.J. Young, R.F. Laine, L. Young, E. Radaelli, I. Benilova, M. Kumar, A. Staes, M. Desager, M. Beerens, P. Vandervoort, A. Luttun, K. Gevaert, G. Bormans, M. Dewerchin, J. Van Eldere, P. Carmeliet, G. Vande Velde, C. Verfaillie, C.F. Kaminski, B. De Strooper, P. Hammarstrom, K.P. Nilsson, L. Serpell, J. Schymkowitz, F. Rousseau, De novo design of a biologically active amyloid, Science 354 (2016).
[9] K.W. Tipping, P. van Oosten-Hawle, E.W. Hewitt, S.E. Radford, Amyloid Fibres: nert end-stage aggregates or key players in disease? Trends Biochem. Sci. 40 (2015) 719–727.
[10] S.I. Cohen, S. Linse, L.M. Luheshi, E. Hellstrand, D.A. White, L. Rajah, D.E. Otzen, M. Vendruscolo, C.M. Dobson, T.P. Knowles, Proliferation of amyloid-beta42 aggregates occurs through a secondary nucleation mechanism, Proc. Natl. Acad. Sci. U. S. A. 110 (2013) 9758–9763.
[11] P. Arosio, T.P. Knowles, S. Linse, On the lag phase in amyloid fibril formation, Phys. Chem. Chem. Phys. 17 (2015) 7606–7618.
[12] J. Bieschke, M. Herbst, T. Wiglenda, R.P. Friedrich, A. Boeddrich, F. Schiele, D. Kleckers, J.M. Lopez del Amo, B.A. Gruning, Q. Wang, M.R. Schmidt, R. Lurz, R. Anwyl, S. Schnoegl, M. Fandrich, R.F. Frank, B. Reif, S. Gunther, D.M. Walsh, E.E. Wanker, Small-molecule

conversion of toxic oligomers to nontoxic beta-sheet-rich amyloid fibrils, Nat. Chem. Biol. 8 (2011) 93–101.
[13] S.A. Sievers, J. Karanicolas, H.W. Chang, A. Zhao, L. Jiang, O. Zirafi, J.T. Stevens, J. Munch, D. Baker, D. Eisenberg, Structure-based design of non-natural amino-acid inhibitors of amyloid fibril formation, Nature 475 (2011) 96–100.
[14] C. Mansson, R.T.P. van Cruchten, U. Weininger, X. Yang, R. Cukalevski, P. Arosio, C.M. Dobson, T. Knowles, M. Akke, S. Linse, C. Emanuelsson, Conserved S/T residues of the human chaperone DNAJB6 are required for effective inhibition of Abeta42 amyloid fibril formation, Biochemistry. 57 (2018) 4891–4902.
[15] P. Pratim Bose, U. Chatterjee, L. Xie, J. Johansson, E. Gothelid, P.I. Arvidsson, Effects of Congo red on abeta(1-40) fibril formation process and morphology, ACS Chem. Neurosci. 1 (2010) 315–324.
[16] A.S. Crystal, B.I. Giasson, A. Crowe, M.P. Kung, Z.P. Zhuang, J.Q. Trojanowski, V.M. Lee, A comparison of amyloid fibrillogenesis using the novel fluorescent compound K114, J. Neurochem. 86 (2003) 1359–1368.
[17] J. Bieschke, J. Russ, R.P. Friedrich, D.E. Ehrnhoefer, H. Wobst, K. Neugebauer, E.E. Wanker, EGCG remodels mature alpha-synuclein and amyloid-beta fibrils and reduces cellular toxicity, Proc. Natl. Acad. Sci. U. S. A. 107 (2010) 7710–7715.
[18] S.I. Cohen, P. Arosio, J. Presto, F.R. Kurudenkandy, H. Biverstal, L. Dolfe, C. Dunning, X. Yang, B. Frohm, M. Vendruscolo, J. Johansson, C.M. Dobson, A. Fisahn, T.P. Knowles, S. Linse, A molecular chaperone breaks the catalytic cycle that generates toxic Abeta oligomers, Nat. Struct. Mol. Biol. 22 (2015) 207–213.
[19] C.E. Bulawa, S. Connelly, M. Devit, L. Wang, C. Weigel, J.A. Fleming, J. Packman, E.T. Powers, R.L. Wiseman, T.R. Foss, I.A. Wilson, J.W. Kelly, R. Labaudiniere, Tafamidis, a potent and selective transthyretin kinetic stabilizer that inhibits the amyloid cascade, Proc. Natl. Acad. Sci. U. S. A. 109 (2012) 9629–9634.
[20] M.S. Maurer, J.H. Schwartz, B. Gundapaneni, P.M. Elliott, G. Merlini, M. Waddington-Cruz, A.V. Kristen, M. Grogan, R. Witteles, T. Damy, B.M. Drachman, S.J. Shah, M. Hanna, D.P. Judge, A.I. Barsdorf, P. Huber, T.A. Patterson, S. Riley, J. Schumacher, M. Stewart, M.B. Sultan, C. Rapezzi, A.-A.S. Investigators, Tafamidis treatment for patients with transthyretin amyloid cardiomyopathy, N. Engl. J. Med. 379 (2018) 1007–1016.
[21] A. Boeddrich, J.T. Babila, T. Wiglenda, L. Diez, M. Jacob, W. Nietfeld, M.R. Huska, C. Haenig, N. Groenke, A. Buntru, E. Blanc, J.C. Meier, E. Vannoni, C. Erck, B. Friedrich, H. Martens, N. Neuendorf, S. Schnoegl, D.P. Wolfer, M. Loos, D. Beule, M.A. Andrade-Navarro, E.E. Wanker, The anti-amyloid compound DO1 decreases plaque pathology and neuroinflammation-related expression changes in 5xFAD transgenic mice, Cell Chem Biol 26 (1) (2019 Jan 17) 109–120, https://doi.org/10.1016/j.chembiol.2018.10.013, e7, Epub 2018 Nov 21.
[22] B.Y. Feng, B.H. Toyama, H. Wille, D.W. Colby, S.R. Collins, B.C. May, S.B. Prusiner, J. Weissman, B.K. Shoichet, Small-molecule aggregates inhibit amyloid polymerization, Nat. Chem. Biol. 4 (2008) 197–199.
[23] D.E. Ehrnhoefer, J. Bieschke, A. Boeddrich, M. Herbst, L. Masino, R. Lurz, S. Engemann, A. Pastore, E.E. Wanker, EGCG redirects amyloidogenic polypeptides into unstructured, off-pathway oligomers, Nat. Struct. Mol. Biol. 15 (2008) 558–566.
[24] S. Giorgetti, S. Raimondi, K. Pagano, A. Relini, M. Bucciantini, A. Corazza, F. Fogolari, L. Codutti, M. Salmona, P. Mangione, L. Colombo, A. De Luigi, R. Porcari, A. Gliozzi, M. Stefani, G. Esposito, V. Bellotti, M. Stoppini, Effect of tetracyclines on the dynamics of formation and destructuration of beta2-microglobulin amyloid fibrils, J. Biol. Chem. 286 (2011) 2121–2131.
[25] L. Lin, N. Mulholland, S.W. Huang, D. Beattie, D. Irwin, Y.C. Gu, J. Clough, Q.Y. Wu, G.F. Yang, Design, synthesis and fungicidal activity of novel sclerotiorin derivatives, Chem. Biol. Drug Des. 80 (2012) 682–692.
[26] T.P. Curtin, J. Reilly, Sclerotiorine, C(20)H(20)O(5)Cl, a chlorine-containing metabolic product of Penicillium sclerotiorum van Beyma, Biochem. J. 34 (1940) 1418 1–1421.
[27] L. Lin, N. Mulholland, Q.Y. Wu, D. Beattie, S.W. Huang, D. Irwin, J. Clough, Y.C. Gu, G.F. Yang, Synthesis and antifungal activity of novel sclerotiorin analogues, J. Agric. Food Chem. 60 (2012) 4480–4491.
[28] C. Chidananda, K.Y. Vasantha, A.P. Sattur, Sclerotiorin is non-mutagenic and inhibits human PMNL 5-lipoxygenase and platelet aggregation, Indian J. Exp. Biol. 53 (2015) 228–231.
[29] H. LeVine 3rd, Thioflavine T interaction with synthetic Alzheimer's disease beta-amyloid peptides: detection of amyloid aggregation in solution, Protein Sci. 2 (1993) 404–410.
[30] H. Oakley, S.L. Cole, S. Logan, E. Maus, P. Shao, J. Craft, A. Guillozet-Bongaarts, M. Ohno, J. Disterhoft, L. Van Eldik, R. Berry, R. Vassar, Intraneuronal beta-amyloid aggregates, neurodegeneration, and neuron loss in transgenic mice with five familial Alzheimer's disease mutations: potential factors in amyloid plaque formation, J. Neurosci. 26 (2006) 10129–10140.
[31] R. Radde, T. Bolmont, S.A. Kaeser, J. Coomaraswamy, D. Lindau, L. Stoltze, M.E. Calhoun, F. Jaggi, H. Wolburg, S. Gengler, C. Haass, B. Ghetti, C. Czech, C. Holscher, P.M. Mathews, M. Jucker, Abeta42-driven cerebral amyloidosis in transgenic mice reveals early and robust pathology, EMBO Rep. 7 (2006) 940–946.
[32] A. Ast, F. Schindler, A. Buntru, S. Schnoegl, E.E. Wanker, A filter retardation assay facilitates the detection and quantification of heat-stable, amyloidogenic mutant huntingtin aggregates in complex biosamples, Methods Mol. Biol. 1780 (2018) 31–40.
[33] M. Biancalana, S. Koide, Molecular mechanism of Thioflavin-T binding to amyloid fibrils, Biochim. Biophys. Acta 1804 (2010) 1405–1412.
[34] B. Bolognesi, J.R. Kumita, T.P. Barros, E.K. Esbjorner, L.M. Luheshi, D.C. Crowther, M.R. Wilson, C.M. Dobson, G. Favrin, J.J. Yerbury, ANS binding reveals common features of cytotoxic amyloid species, ACS Chem. Biol. 5 (2010) 735–740.
[35] W. Huber, A new strategy for improved secondary screening and lead optimization using high-resolution SPR characterization of compound-target interactions, J. Mol. Recogn. 18 (2005) 273–281.
[36] C. Raingeval, O. Cala, B. Brion, M. Le Borgne, R.E. Hubbard, I. Krimm, 1D NMR WaterLOGSY as an efficient method for fragment-based lead discovery, J. Enzym. Inhib. Med. Chem. 34 (2019) 1218–1225.
[37] T. Aoyama, Y. Murase, T. Iwata, A. Imaizumi, Y. Suzuki, Y. Sato, Comparison of blood-free medium (cyclodextrin solid medium) with Bordet-Gengou medium for clinical

isolation of Bordetella pertussis, J. Clin. Microbiol. 23 (1986) 1046–1048.
[38] O. Cala, F. Guilliere, I. Krimm, NMR-based analysis of protein-ligand interactions, Anal. Bioanal. Chem. 406 (2014) 943–956.
[39] W. Hoffmann, G. von Helden, K. Pagel, Ion mobility-mass spectrometry and orthogonal gas-phase techniques to study amyloid formation and inhibition, Curr. Opin. Struct. Biol. 46 (2017) 7–15.
[40] S.L. Bernstein, N.F. Dupuis, N.D. Lazo, T. Wyttenbach, M.M. Condron, G. Bitan, D.B. Teplow, J.E. Shea, B.T. Ruotolo, C.V. Robinson, M.T. Bowers, Amyloid-beta protein oligomerization and the importance of tetramers and dodecamers in the aetiology of Alzheimer's disease, Nat. Chem. 1 (2009) 326–331.
[41] L.M. Young, J.C. Saunders, R.A. Mahood, C.H. Revill, R.J. Foster, L.H. Tu, D.P. Raleigh, S.E. Radford, A.E. Ashcroft, Screening and classifying small-molecule inhibitors of amyloid formation using ion mobility spectrometry-mass spectrometry, Nat. Chem. 7 (2015) 73–81.
[42] X. Zheng, D. Liu, F.G. Klarner, T. Schrader, G. Bitan, M.T. Bowers, Amyloid beta-protein assembly: the effect of molecular tweezers CLR01 and CLR03, J. Phys. Chem. B 119 (2015) 4831–4841.
[43] A.C. Susa, C. Wu, S.L. Bernstein, N.F. Dupuis, H. Wang, D.P. Raleigh, J.E. Shea, M.T. Bowers, Defining the molecular basis of amyloid inhibitors: human islet amyloid polypeptide-insulin interactions, J. Am. Chem. Soc. 136 (2014) 12912–12919.
[44] S.J.C. Lee, T.S. Choi, J.W. Lee, H.J. Lee, D.G. Mun, S. Akashi, S.W. Lee, M.H. Lim, H.I. Kim, Structure and assembly mechanisms of toxic human islet amyloid polypeptide oligomers associated with copper, Chem. Sci. 7 (2016) 5398–5406.
[45] W. Hoffmann, K. Folmert, J. Moschner, X. Huang, H. von Berlepsch, B. Koksch, M.T. Bowers, G. von Helden, K. Pagel, NFGAIL amyloid oligomers: the onset of beta-sheet formation and the mechanism for fibril formation, J. Am. Chem. Soc. 140 (2018) 244–249.
[46] J. Seo, W. Hoffmann, S. Warnke, X. Huang, S. Gewinner, W. Schollkopf, M.T. Bowers, G. von Helden, K. Pagel, An infrared spectroscopy approach to follow beta-sheet formation in peptide amyloid assemblies, Nat. Chem. 9 (2017) 39–44.
[47] S. Jin, N. Kedia, E. Illes-Toth, I. Haralampiev, S. Prisner, A. Herrmann, E.E. Wanker, J. Bieschke, Amyloid-beta(1-42) aggregation initiates its cellular uptake and cytotoxicity, J. Biol. Chem. 291 (2016) 19590–19606.
[48] M.V. Berridge, P.M. Herst, A.S. Tan, Tetrazolium dyes as tools in cell biology: new insights into their cellular reduction, Biotechnol. Annu. Rev. 11 (2005) 127–152.
[49] G.T. Heller, P. Sormanni, M. Vendruscolo, Targeting disordered proteins with small molecules using entropy, Trends Biochem. Sci. 40 (2015) 491–496.
[50] T.M. Ryan, A. Friedhuber, M. Lind, G.J. Howlett, C. Masters, B.R. Roberts, Small amphipathic molecules modulate secondary structure and amyloid fibril-forming kinetics of Alzheimer disease peptide Abeta(1-42), J. Biol. Chem. 287 (2012) 16947–16954.
[51] T.M. Ryan, M.D. Griffin, C.L. Teoh, J. Ooi, G.J. Howlett, High-affinity amphipathic modulators of amyloid fibril nucleation and elongation, J. Mol. Biol. 406 (2011) 416–429.
[52] S.R. Paranjape, A.P. Riley, A.D. Somoza, C.E. Oakley, C.C. Wang, T.E. Prisinzano, B.R. Oakley, T.C. Gamblin, Azaphilones inhibit tau aggregation and dissolve tau aggregates in vitro, ACS Chem. Neurosci. 6 (2015) 751–760.
[53] G.T. Heller, F.A. Aprile, M. Bonomi, C. Camilloni, A. De Simone, M. Vendruscolo, Sequence specificity in the entropy-driven binding of a small molecule and a disordered peptide, J. Mol. Biol. 429 (2017) 2772–2779.
[54] G. Fusco, M. Sanz-Hernandez, F.S. Ruggeri, M. Vendruscolo, C.M. Dobson, A. De Simone, Molecular determinants of the interaction of EGCG with ordered and disordered proteins, Biopolymers 109 (2018) e23117.
[55] J. Bieschke, Natural compounds may open new routes to treatment of amyloid diseases, Neurotherapeutics 10 (2013) 429–439.
[56] F. Ferrone, Analysis of protein aggregation kinetics, Methods Enzymol. 309 (1999) 256–274.
[57] R. Riek, D.S. Eisenberg, The activities of amyloids from a structural perspective, Nature 539 (2016) 227–235.
[58] P. Mishra, S.R. Ayyannan, G. Panda, Perspectives on inhibiting beta-amyloid aggregation through structure-based drug design, ChemMedChem 10 (2015) 1467–1474.
[59] N. Osterlund, Y.S. Kulkarni, A.D. Misiaszek, C. Wallin, D.M. Kruger, Q. Liao, F. Mashayekhy Rad, J. Jarvet, B. Strodel, S. Warmlander, L.L. Ilag, S.C.L. Kamerlin, A. Graslund, Amyloid-beta peptide interactions with amphiphilic surfactants: electrostatic and hydrophobic effects, ACS Chem. Neurosci. 9 (2018) 1680–1692.
[60] F.L. Palhano, J. Lee, N.P. Grimster, J.W. Kelly, Toward the molecular mechanism(s) by which EGCG treatment remodels mature amyloid fibrils, J. Am. Chem. Soc. 135 (2013) 7503–7510.
[61] I. Horvath, C.F. Weise, E.K. Andersson, E. Chorell, M. Sellstedt, C. Bengtsson, A. Olofsson, S.J. Hultgren, M. Chapman, M. Wolf-Watz, F. Almqvist, P. Wittung-Stafshede, Mechanisms of protein oligomerization: inhibitor of functional amyloids templates alpha-synuclein fibrillation, J. Am. Chem. Soc. 134 (2012) 3439–3444.
[62] A.K.R. Dasari, R.M. Hughes, S. Wi, I. Hung, Z. Gan, J.W. Kelly, K.H. Lim, Transthyretin aggregation pathway toward the formation of distinct cytotoxic oligomers, Sci. Rep. 9 (2019) 33.
[63] R. Ahmed, M. Akcan, A. Khondker, M.C. Rheinstadter, J.C. Bozelli Jr., R.M. Epand, V. Huynh, R.G. Wylie, S. Boulton, J. Huang, C.P. Verschoor, G. Melacini, Atomic resolution map of the soluble amyloid beta assembly toxic surfaces, Chem. Sci. 10 (2019) 6072–6082.
[64] S. Hilt, R. Altman, T. Kalai, I. Maezawa, Q. Gong, S. Wachsmann-Hogiu, L.W. Jin, J.C. Voss, A bifunctional anti-amyloid blocks oxidative stress and the accumulation of intraneuronal amyloid-beta, Molecules 23 (2018).
[65] A. Jan, O. Adolfsson, I. Allaman, A.L. Buccarello, P.J. Magistretti, A. Pfeifer, A. Muhs, H.A. Lashuel, Abeta42 neurotoxicity is mediated by ongoing nucleated polymerization process rather than by discrete Abeta42 species, J. Biol. Chem. 286 (2011) 8585–8596.
[66] L. Pieri, K. Madiona, L. Bousset, R. Melki, Fibrillar alpha-synuclein and huntingtin exon 1 assemblies are toxic to the cells, Biophys. J. 102 (2012) 2894–2905.
[67] L.A. Volpicelli-Daley, K.C. Luk, T.P. Patel, S.A. Tanik, D.M. Riddle, A. Stieber, D.F. Meaney, J.Q. Trojanowski, V.M. Lee, Exogenous alpha-synuclein fibrils induce Lewy

body pathology leading to synaptic dysfunction and neuron death, Neuron 72 (2011) 57–71.
[68] P. Arosio, M. Vendruscolo, C.M. Dobson, T.P. Knowles, Chemical kinetics for drug discovery to combat protein aggregation diseases, Trends Pharmacol. Sci. 35 (2014) 127–135.
[69] V. Sklenar, M. Piotto, R. Leppik, V. Saudek, Gradient-tailored water suppression for 1H-15N HSQC experiments optimized to retain full sensitivity, J. Magn. Reson., Ser. A 102 (1993) 241–245.
[70] T.L. Hwang, A.J. Shaka, Water suppression that works. Excitation sculpting using arbitrary wave-forms and pulsed-field gradients, J. Magn. Reson., Ser. A 112 (1995) 275–279.
[71] G. Bodenhausen, D.J. Ruben, Natural abundance nitrogen-15 NMR by enhanced heteronuclear spectroscopy, Chem. Phys. Lett. 69 (1980) 185–189.
[72] P. Schanda, E. Kupce, B. Brutscher, SOFAST-HMQC experiments for recording two-dimensional heteronuclear correlation spectra of proteins within a few seconds, J. Biomol. NMR 33 (2005) 199–211.
[73] C. Dalvit, P. Pevarello, M. Tato, M. Veronesi, A. Vulpetti, M. Sundstrom, Identification of compounds with binding affinity to proteins via magnetization transfer from bulk water, J. Biomol. NMR 18 (2000) 65–68.
[74] J. Roche, Y. Shen, J.H. Lee, J. Ying, A. Bax, Monomeric abeta(1-40) and abeta(1-42) peptides in solution adopt very similar ramachandran map distributions that closely resemble random coil, Biochemistry 55 (2016) 762–775.
[75] S.J. Allen, K. Giles, T. Gilbert, M.F. Bush, Ion mobility mass spectrometry of peptide, protein, and protein complex ions using a radio-frequency confining drift cell, Analyst 141 (2016) 884–891.
[76] H.E. Revercomb, E.A. Mason, Theory of plasma chromatography gaseous electrophoresis – review, Anal. Chem. 47 (1975) 970–983.